International Journal of Water Resources and Environmental Engineering

Volume 9 Number 4 April 2017

ISSN-2141-6613

Academic Journals

ABOUT IJWREE

The International Journal of Water Resources and Environmental Engineering is published monthly (one volume per year) by Academic Journals.

International Journal of Water Resources and Environmental Engineering (IJWREE) is an open access journal that provides rapid publication (monthly) of articles in all areas of the subject such as water resources management, waste management, ozone depletion, Kinetic Processes in Materials, strength of building materials, global warming etc. The Journal welcomes the submission of manuscripts that meet the general criteria of significance and scientific excellence. Papers will be published shortly after acceptance. All articles published in IJWREE are peer-reviewed.

Contact Us

Editorial Office: ijwree@academicjournals.org

Help Desk: helpdesk@academicjournals.org

Website: http://www.academicjournals.org/journal/IJWREE

Submit manuscript online http://ms.academicjournals.me/

Editors

Editorial Board

International Journal of Water Resources and Environmental Engineering

Table of Contents: Volume 9 Number 4 April 2017

ARTICLES

academicJournals

Vol. 9(4), pp. 72-85, April 2017
DOI: 10.5897/IJWREE2017.0710
Article Number: A84C52663408
ISSN 2141-6613

http://www.academicjournals.org/IJWREE

International Journal of Water Resources and Environmental Engineering

Full Length Research Paper

Geostatistical study of the spatial variability of groundwater parameters in Afikpo and Ohaozara, Southeastern Nigeria

Robert Egwu Otu Iduma[1]*, Tamunoene Kingdom Simeon Abam[2] and Etim Daniel Uko[3]

[1]Groundscan Services Nig. Ltd., Port-Harcourt, Rivers State, Nigeria.
[2]Institute of Geosciences and Space Technology, Rivers State University of Science and Technology, Port Harcourt, Rivers State, Nigeria.
[3]Department of Physics, Rivers State University of Science and Technology, Port Harcourt, Rivers State, Nigeria.

Received 19 January, 2017; Accepted 1 March, 2017

Abortive boreholes and parched wells, ascribed to the difficulty in understanding the hydrogeology of the aquifer by water borehole drillers, pose great concern to the people of the region. Mapping the spatial variability of water table depth (WTD) (m) and aquifer thickness H (m) is a vital step in optimal utilization of groundwater resources. Thus, the aim of this paper is to investigate the spatial variability of the groundwater parameters, H (m) and WTD (m) in the study area located in Nigeria, using geostatistical method of Ordinary Kriging, based on data estimated from interpreted results of fifty (50) Schlumberger Vertical Electrical Sounding (VES) curves. To attain this aim, the spatial variability of the groundwater parameters was analyzed. The result shows that the difference in directional behavior is not significant. Thus, the WTD and H were assumed as isotropic, and experimental semivariograms of logH and log(WTD) were calculated and modeled with the GS$^+$ software. It was found that, H and (WTD) data are moderately spatially correlated over the study area, and the spatial structures follow exponential model for H and spherical model for (WTD). According to the generated maps of kriged estimates of logH and log(WTD), the southern part of the study area with higher prolific aquiferous zone, shows higher kriged H-values, relative to the northern zone. The variation in the distribution of kriged WTD-values in the study region is asymmetrical. These results compare favorably in the trend patterns of distribution of the parameter values, with contour maps of a previous study in the region that indicates the distribution of H and WTD parameters. The parameters of the semivariogram models used for the analysis of the data, give insight into the spatial pattern of the groundwater parameters, H and WTD. This knowledge has improved the ability to understand the hydrogeology of the aquifer. The generated spatial variability maps of H and WTD will assist water resource managers and policymakers in the development of guidelines in judicious management of groundwater resources for drinking purposes in the study area.

Key words: Ordinary kriging, Aquifer thickness, water table depth, semivariogram, exponential model, spherical model, cross-validation.

INTRODUCTION

In recent years, the importance of groundwater as a natural resource has been increasingly recognized throughout the world. But, population growth in the study area has resulted in expanding residential developments

and consequently, increased demand for water, resulting in lowering of the groundwater water table due to excessive withdrawals.

Keeping the water table at a favorable level is quite significant. When a well is placed in an aquifer, lowering the water table will not only have an effect on the thickness of the aquifer, but can also cause salt water from the ocean to move further inland, acting as a contaminant to aquifers. As the water table becomes too low to be tapped from, the expensive wells are abandoned as unproductive or desiccated wells. Therefore, it is very important to estimate the spatial distribution pattern of the groundwater aquifer parameters in order to boost the ability to understand the fluctuations in water table depth due to extraction and the hydrogeology of the aquifer. Using geostatistics, it is possible to map the spatial variability of the aquifer parameters and improve the qualitative and quantitative management of water resources. This has been described further with literature review. For example, Ahmadi and Sedghamiz (2007) evaluated kriging and cokriging methods for mapping the groundwater depth across a plain in which there has been different climatic conditions (dry, wet, and normal). Results obtained from geostatistical analysis showed that groundwater depth varied spatially in different climatic conditions. Yang et al. (2008) discussed the kriging approach combined with hydrogeological analysis (based on GIS) for the design of groundwater level monitoring network. The effect of variogram parameters (that is, the sill, nugget effect and range) on network was analyzed. In their efforts to analyze the spatial variability of groundwater depth and quality parameters, Dash et al. (2010), used ordinary kriging and indicator kriging to generate spatial variability maps in the National Capital Territory of Delhi, India. The results indicated that in 43% of the study area, groundwater depth was within 20 m. The salinity level was higher than 2.5 ds m^{-1} in 69% of the study area. Also, Andarge et al. (2013), estimated transmissivity using empirical and geostatistical methods in the volcanic aquifers of Upper Awash Basin, Central Ethiopia. They performed linear and logarithmic regression functions and it was found that the logarithmic relationship predicting transmissivity from specific capacity data has a better correlation (R = 0.97) than the linear relationship (R = 0.79). Masoomeh et al. (2013), investigated the spatio-temporal variability of groundwater quality parameters (Electrical Conductivity, Sodium Adsorption Ratios, Total Dissolved Solids, and Sodium content) using geostatistics and GIS in Shiraz City, South Iran. Results revealed that ground water quality data are strongly spatially correlated over the study region.

Pradipika and Surya (2014) studied the spatial variability of ground water depth and quality parameter in Haridwar District of Uttarakhand, using ordinary kriging. It was observed that the semivariogram parameters fitted well in the spherical model for water depth, and in the exponential model for water quality parameter. Both parameters followed a log-normal distribution and demonstrated a moderate spatial dependence according to the nugget ratio. Other similar studies have shown that geostatistical approach is a suitable method for estimation of aquifer hydraulic properties (Doctor and Nelson, 1981; Sophocleous et al., 1982; Nunes et al., 2004a; Arslan, 2012, 2013; Rawat et al., 2012; Varouchakis et al., 2012; Delbari, 2013). Thus, to achieve the purpose of this study, the core objectives consists of variographic analysis of the spatial variability of groundwater parameters H and WTD, the generation of maps of kriged estimates of logH and log(WTD), and back transforms of logH and log(WTD) to H and WTD to assess the H and WTD fields.

Description of study area

The study area falls within Southeastern Nigeria in the Afikpo Basin, bounded by Long. 7° 45′E to 8° 00′E and Lat. 5° 43′N to 5° 57′N (in Nigerian local datum) and traverses two regions; the Ohaozara area and Afikpo province-consisting of Amasiri, Ozziza, and Unwana, covering an area of about 607.75 km^2 (Figure 1). The area lies mostly in the (Eboine) River Basin and the Cross River plains on the south-eastern flank of the Abakaliki-Benue anticlinorium (Figure 2a). The area has an undulating terrain and an elevation of about 170 m above mean sea level. Remarkably, sandstone forms its ridges and the shale forms the valley. The shale unit underlies the bioturbated sandstone. These bioturbated sandstones have very high altitude; this is possibly because they have less period of exposure to erosion.

Geology and hydrogeology of the study area

Geologically, the area falls within the Cretaceous Abakaliki-Benue Rift (Figure 2a), and is underlain by the Asu River Group (Albian), the Turonian Eze-Aku formation and the (Late Campanian-Early Maastrichtian) Nkporo formation. The Turonian Amasiri sandstone of the Eze-Aku group is a highly consolidated, well cemented, subangular to subrounded, poorly sorted, very fine to medium grained feldspathic arenite with poor reservoir quality (Okereke, 2012). This unit dominates the northern

*Corresponding author. E-mail: bob_idu@yahoo.com.

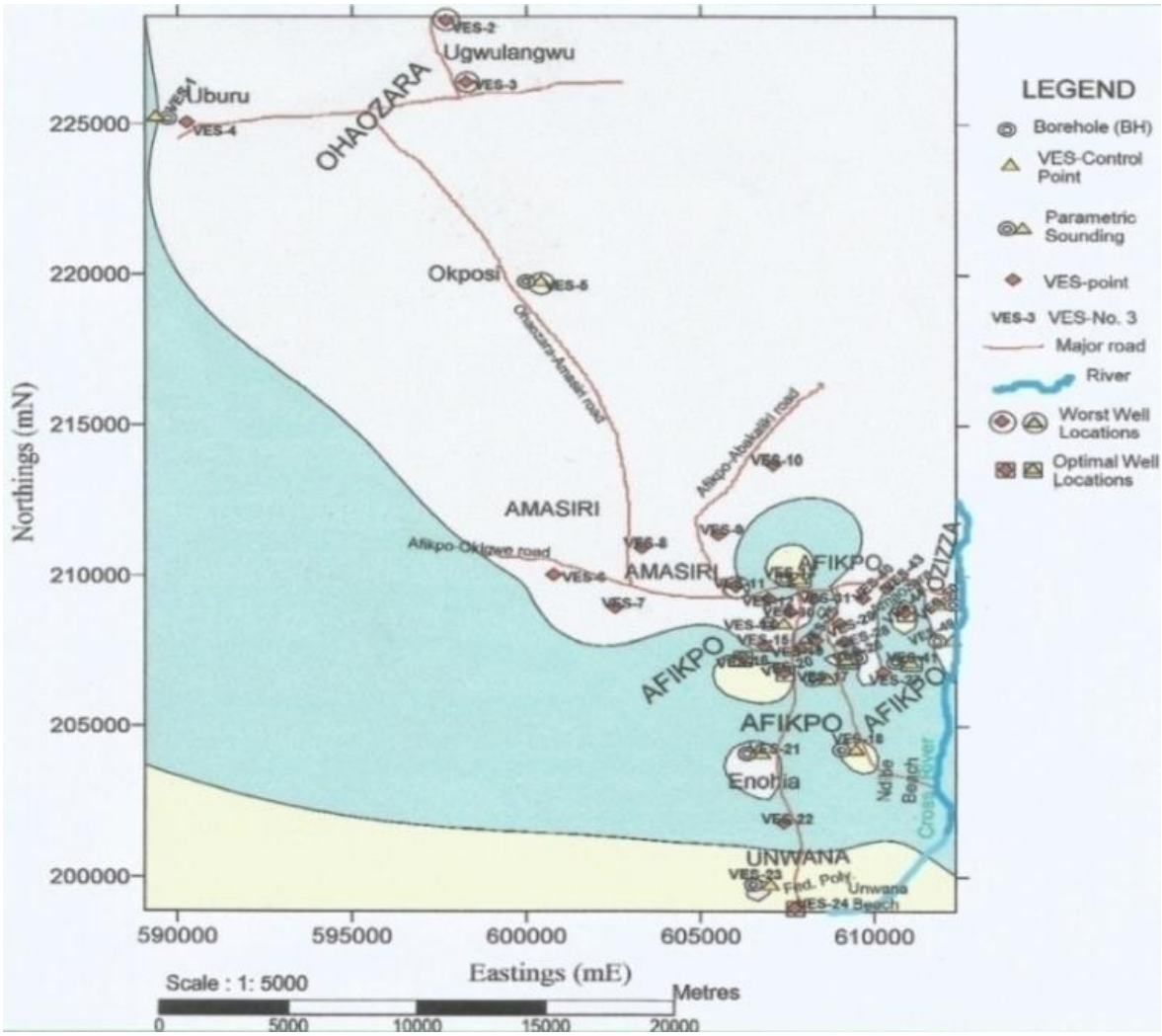

Figure 1. Showing the study area with access roads, VES stations, and Borehole points (Iduma et al., 2016).

parts of the study area. Local geology of the study area indicates that extensive marine transgression and regression occurred in the Turonian followed by the period of Orogeny during the Coniancian, especially the Santonian. Contemporaneous with the Orogeny was the intrusion of the igneous bodies described as dolerite sills, into the Eze-Aku Shale (Okonkwo et al., 2013; Obiora, 2002). The geological map of the study area is as shown in Figure 2b.

The Nkporo Formation is the basal lithostratigraphic unit of the Afikpo sub-basin and comprises dominantly of dark grey to black shales, sandstone, minor limestone and oolitic ironstone beds. In the Campanian-Maastrichtian, there was subsidence and a marine regression resulted in the deposition of a lateral equivalent to Nkporo Formation named Afikpo Sandstone. Simpson (1954), Reyment (1965) and Whiteman (1982) reported the presence of an angular unconformity between the Campanian-Maastrichtian Afikpo Sandstone and the Turonian Eze-Aku group. The Afikpo Sandstone is the youngest sedimentary unit in the study area. Its relatively loose structure, coarse grains, sorting enables it to be porous and permeable. The formation covers most parts of Afikpo town, hence the name, Afikpo Sandstone.

Shale and sandstone are the two major lithologic units in the area. The sandstone units constitute the permeable and saturated aquifers. The dominant lithology in the southern zone of the study is the Afikpo sandstone. Almost, the entire northern area is underlain by well compacted, hard Amasiri Sandstone of the Santonian Eze-Aku group. The nature of this unit obviously reduces infiltration unless in parts that are fractured or deeply weathered. It is possible that the regional Cretaceous tectonic activity shattered the rocks of the area after the deposition of the sediments. Hence, places that exhibit intense fracturing yield water at shallow depth (Simpson, 1955).

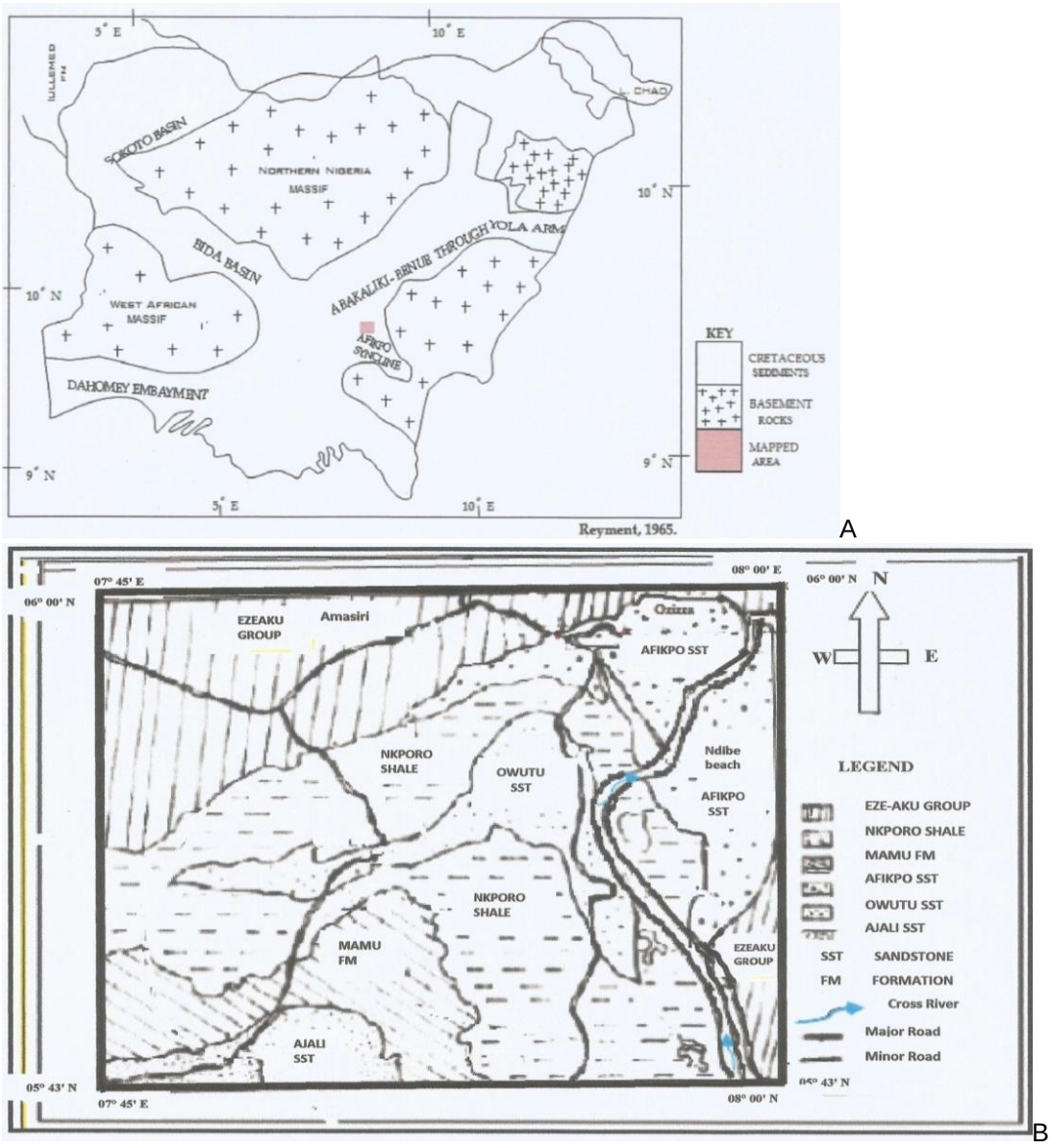

Figure 2. (a) Map of Nigeria showing the distribution of cretaceous sediments; (b) Map showing geological map of the study area (Iduma et al., 2016).

METHODOLOGY

The geostatistical study is based on data estimated from interpreted results of fifty (50) Schlumberger Vertical Electrical Sounding (VES) curves with maximum current electrode spacing of AB/2 = 681 m. The details of the geoelectrical data acquisition, processing, and interpretation methods, are contained in Iduma (2014). For effective use of the geoelectrical data in the geostatistical study, the validity of the resistivity data was tested in a borehole-lithology and geoelectrical-column correlations. The H and WTD data values computed from the VES data are shown in Table 1. The procedures adopted in the correlation attempt are explained in Iduma et al. (2016).

Most often, skewed or erratic data can be made more suitable for geostatistical modeling by appropriate transformation. Ordinary kriging is well-known to be optimal when the data have a multivariate normal distribution. Transformation of data therefore may be required before kriging to normalize the data distribution, suppress outliers and improve data stationarity (Deutsch and Journel, 1992; Armstrong, 1989). The estimation then is performed in the Gaussian domain before back-transforming the estimates to the original domain. The Gaussian distribution has the advantage that spatial variability is easier to be modeled because it reduces the effects of extreme values providing more stable variograms (Goovaerts, 1997; Armstrong, 1989). In this study, geostatistical analysis of the data is accomplished using the software GS^+ Ver. 10.0 (Gamma Design Software, Plainwell, USA). Fifty (50) aquifer thickness (H) and water table depth (WTD) data (Table 1), estimated from the interpretation of VES data were used as input data for the geostatistical study. Kriging represents variability only up to the second order moment (covariance), so the random field of the transformed variable must therefore be Gaussian to derive

Table 1. Interpreted results of vertical electrical sounding in the study area.

VES No.	Easting (mE)	Northing (mN)	H (m)	WTD (m)
1	589069.364	225241.733	89.78	2.43
2	597541.102	228572.138	40.3	7.42
3	598036.634	226470.968	39.99	32.56
4	590068.517	225145.188	23.83	12.35
5	600242.627	219835.01	61.11	15.79
6	600625.099	210096.49	61.67	8.06
7	602315.315	208958.34	47.7	8.62
8	603111.515	210993.516	27.43	4.52
9	605233.508	211476.439	36.09	40.12
10	606828.818	213691.99	38.63	11.81
11	605754.414	209670.17	50.17	3.73
12	606688.941	209294.541	71.00	21.21
13	607615.361	209993.765	154.1	8.22
14	607167.925	208535.525	29.38	1.6
15	606588.987	207749.96	37.37	2.55
16	605958.003	207331.47	112.72	10.14
17	608534.698	206725.36	54.55	4.12
18	609298.081	204264.789	113.9	13.4
19	607606.803	207629.151	45.08	9.15
20	607160.08	206871.084	139.58	17.82
21	606594.353	204049.471	49.59	2.9
22	607167.245	201825.528	68.28	2.65
23	606765.319	199789.908	151.68	18.52
24	607499.532	198870.958	130.6	34.3
25	608059.173	207898.935	157	7.61
26	608993.471	207246.962	147.45	46.35
27	609629.732	206871.68	52.48	35.59
28	608821.836	207842.893	33.11	6.2
29	608733.068	208264.006	58.71	5.59
30	607392.706	208793.254	43.9	3.86
31	607971.364	209262.519	30.66	31.47
32	608057.208	208998.332	40.02	3.42
33	607832.145	208448.862	45.94	11.9
34	608671.909	208613.847	59.52	9.23
35	608531.455	209627.396	64.98	32.66
36	608112.219	208654.331	47.81	16.49
37	608536.7	208798.238	162.1	31.59
38	609099.843	209064.847	37.79	9.41
39	609250.253	208776.03	32.2	9.12
40	609628.906	209156.451	41.27	1.77
41	610891.026	207214.397	100.47	11.79
42	609738.962	208487.157	28.34	8.92
43	610339.756	209597.968	57.9	7.46
44	610889.469	208789.781	165.9	91.48
45	609857.616	207172.407	52.29	25.79
46	611578.48	208911.957	35.29	4.03
47	612322.756	208938.89	44.64	5.2
48	612315.856	208143.529	32.7	1.39
49	612060.318	207852.033	38.68	4.48
50	611643.342	209203.632	51.74	1.55

Table 2. Summary statistics of groundwater parameters, H and WTD.

Parameter	Mean	Minimum	Maximum	Standard deviation	Skewness coefficient
H (m)	66.748	23.83	165.90	42.164	1.25
LogH	4.041	3.17	5.11	0.541	0.68
WTD (m)	14.367	1.39	91.48	16.011	2.63
Log (WTD)	2.191	0.33	4.52	0.992	0.09

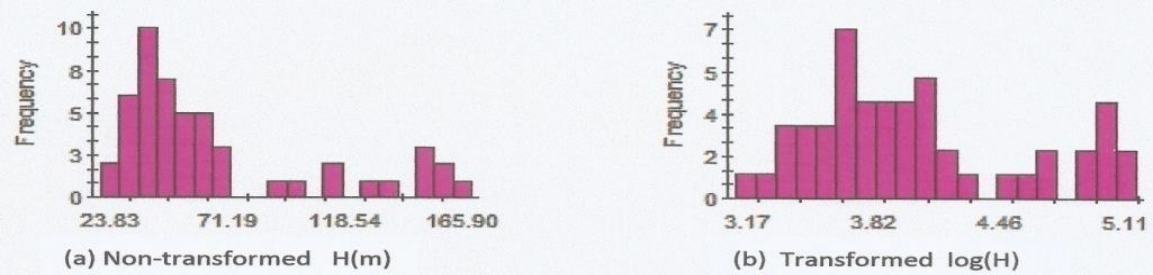

Figure 3. Frequency distribution of (a) non-transformed and (b) transformed aquifer thickness H(m).

unbiased estimates at non-sampled locations (Deutsch and Journel, 1992; Goovaerts et al., 2005). A non-linear normalizing data transformation (log transformation) is applied in union with kriging for the accurate prediction of spatial variability of the groundwater parameters under study. A cross-validation (Isaaks and Srivastava, 1989) approach is used to assess the performance and interpolation errors of ordinary kriging in the estimation of groundwater parameters (H and WTD). The comparison criteria used are coefficient of determination (R^2) and residual sum of squares (RSS). For appropriate estimator, R^2 should be close to 1 and RSS should be as small as possible (Robertson, 2008). In this study, it is assumed that: (1) all values of (H) and WTD data, in the study area are the results of a random process, with dependence (spatial autocorrelation) and (2) the variance of the difference is the same between any two points that are at the same distance apart and direction, no matter which two points are chosen (stationarity assumption).

The theory of geostatistics and principles of kriging have been well documented previously (Isaaks and Srivastava, 1989; Goovaerts, 1997; David, 1977; Journel and Huijbregts, 1978; Kitanidis, 1997) and will not be repeated in this paper. Interested readers are referred to these cited references. More advanced treatment of the subject can also be found in Webster and Oliver (2001).

RESULTS

Statistical analysis of H and WTD data has been presented. Spatial variability analysis and model fitting have been done. The results also include cross-validation and spatial prediction of H and WTD data, and mapped values of H and WTD with estimation variance maps.

Statistical analysis of H and WTD data

Table 2 provides descriptive statistics for H and WTD data. The available raw data range between 165.90 to 23.83 m and 91.48 to 1.39 m for H and WTD data, respectively, straddling several orders of magnitude. The mean values of H and WTD data are correspondingly, 66.748 and 14.367 m. To preserve a certain continuity of the data, some data values (outliers) were isolated relative to the entire data, in the cross-validation procedure. Figures 3b and 4b show the frequency distributions of logH and log(WTD), respectively, and indicate a fairly normal distribution relative to the untransformed, H and WTD data. The frequency distribution of the untransformed data is shown in Figures 3a and 4a. The frequency distribution of the transformed data is positively skewed with a symmetrical form. The skewness coefficient of transformed data (Table 2, column 6) is much less than those of real data. So, the data are transformed using a log transformation function. A comparison of standard deviation for log transformed data with the untransformed data for both parameters indicates that a reduction in prediction standard deviation would occur if log transformed H and WTD values are estimated against the untransformed data.

Spatial variability analysis and model fitting

To investigate the spatial variability of groundwater parameters, experimental semivariograms of logH and log (WTD), are calculated for four directions (0, 45, 90 and 135°) with an angle tolerances of 22.5°. The results (Figure 5a and b), did not show any significance differences, that is, no significant anisotropy, hence, the investigated parameters are assumed to be isotropic, and omnidirectional semivariograms is calculated for each of

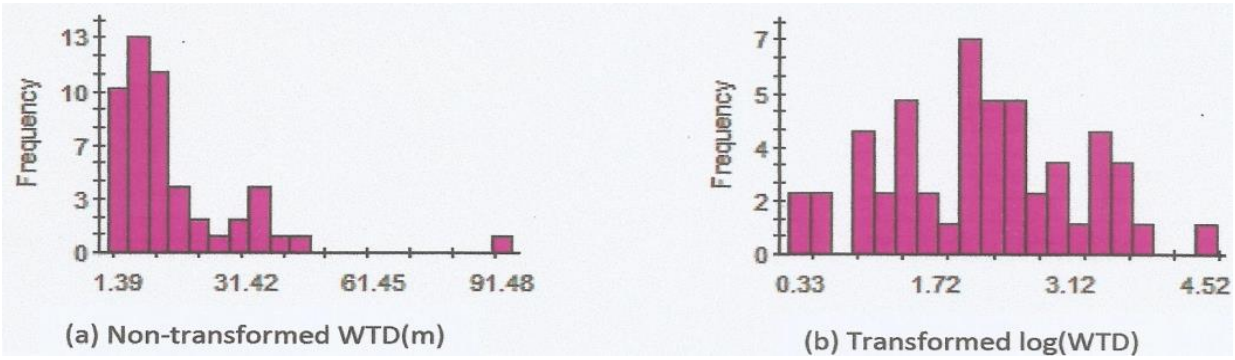

Figure 4. Frequency distribution of (a) non-transformed and (b) transformed water table depth WTD(m).

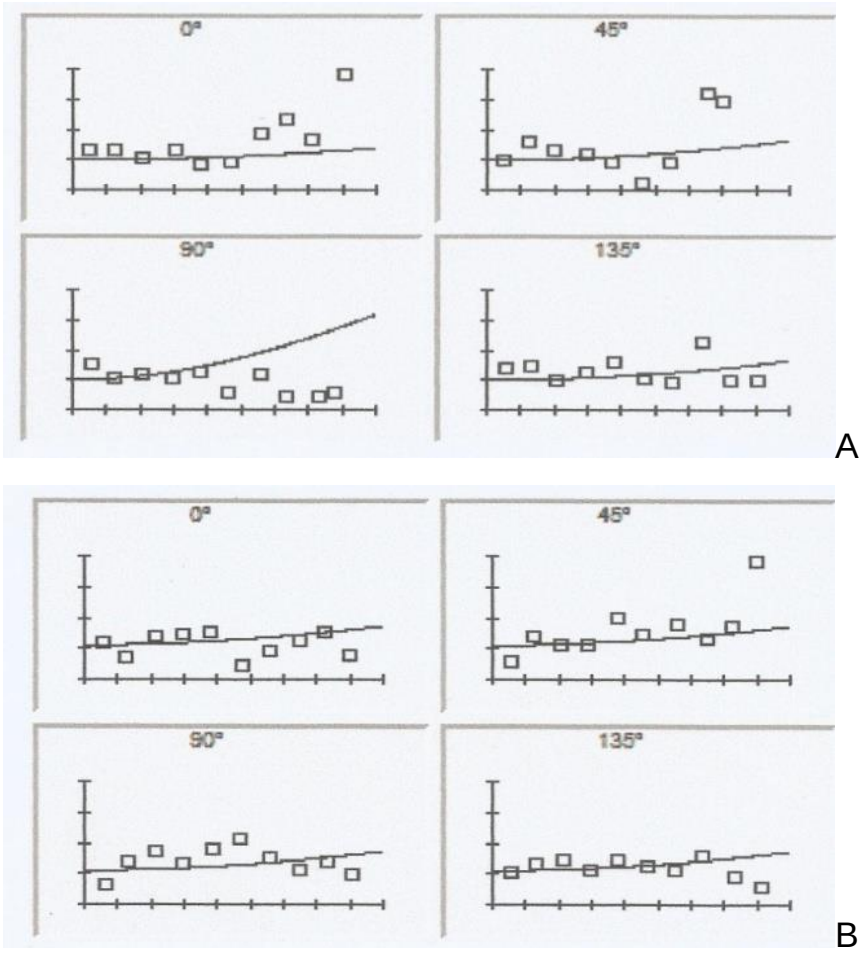

Figure 5. (a) Anistropic variograms for logH data showing spatial variability analysis for four directions; (b) Anistropic variograms for log(WTD) data showing spatial variability analysis for four directions.

them. Then the best semivariogram model is fitted to the experimental data. The model depends on the choice of three parameters: nugget, sill, and range parameters. The model fitting is done by defining a curve that provides the best fit through the points in the empirical semivariogram graph by ensuring that the squared difference (RSS) between the data points and the curve is minimum (Robertson, 2008). Spherical, Exponential, and Gaussian

Table 3. Characteristics of semivariogram models for groundwater parameters.

Parameter	Model type	C_0	$C_0 + C$	$(C_0 / C_0 + C)$	Range parameter	Coefficient of variation (CV)	R^2	RSS
	Exponential	0.2300	0.8020	0.2867	31100	0.327	0.572	0.0637
H	Gaussian	0.0783	0.33660	0.2326	600	0.008	0.089	.0939
	Spherical	0.0504	0.33680	0.1496	1230	0.008	0.089	0.0939
	Exponential	0.1430	1.04100	0.1374	500	0.381	0.617	0.2050
WTD	Gaussian	0.1840	1.03000	0.1786	540	0.378	0.615	0.2060
	Spherical	0.2360	1.03600	0.2278	1370	0.392	0.626	0.2010

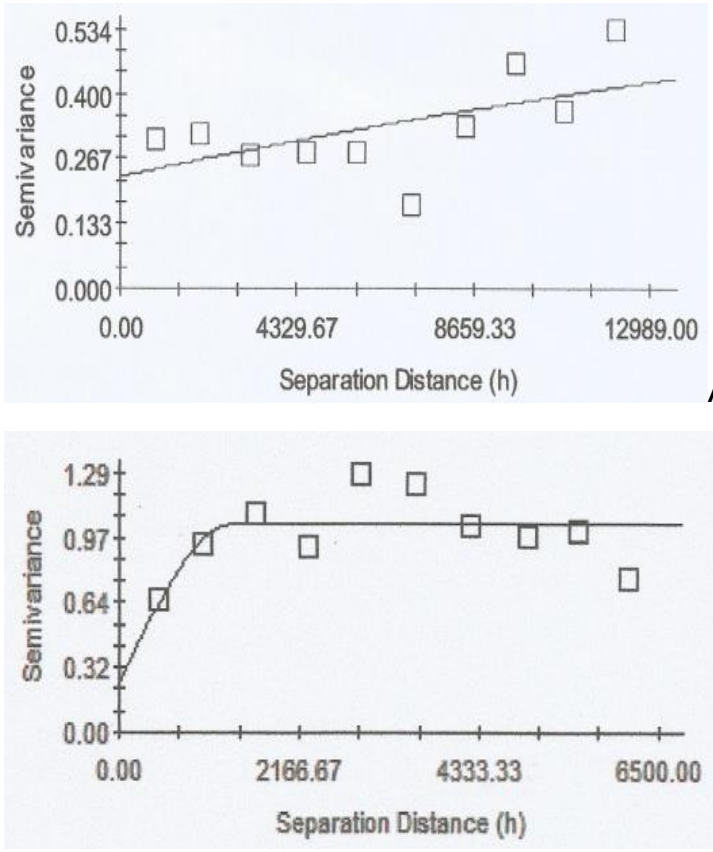

Figure 6. (a) Fitted model (Exponential model) to logH exponential semivariogram; (b) Fitted model (Spherical model) to log(WTD) exponential semivariogram.

functions were fitted, one at a time, to the empirical data for evaluation. The best model, in bold letters (Table 3, column 2), is the one that has the least RSS and largest coefficient of variation (C.V), which is the square of correlation coefficient (R^2). Semivariogram model characteristics for each parameter (H, WTD) are shown in Table 3. The fitting models to logH and log WTD experimental semivariograms are as shown in Figure 6a and b, respectively. As recommended by Mehrjardi et al. (2008), when the ratio $C_0 / (C_0 + C)$ in Table 3, is less than 0.25, the variable has a strong spatial correlation, if the ratio $C_0 / (C_0 + C)$ is greater than 0.25 and less 0.75, the variable has a moderate spatial correlation, but, when the ratio $C_0 / (C_0 + C)$ is greater than 0.75, the variable is said to have a weak spatial correlation.

The results indicate that spatial structure of both variables, H and WTD, are moderate and follow an exponential model for the H data and spherical model for

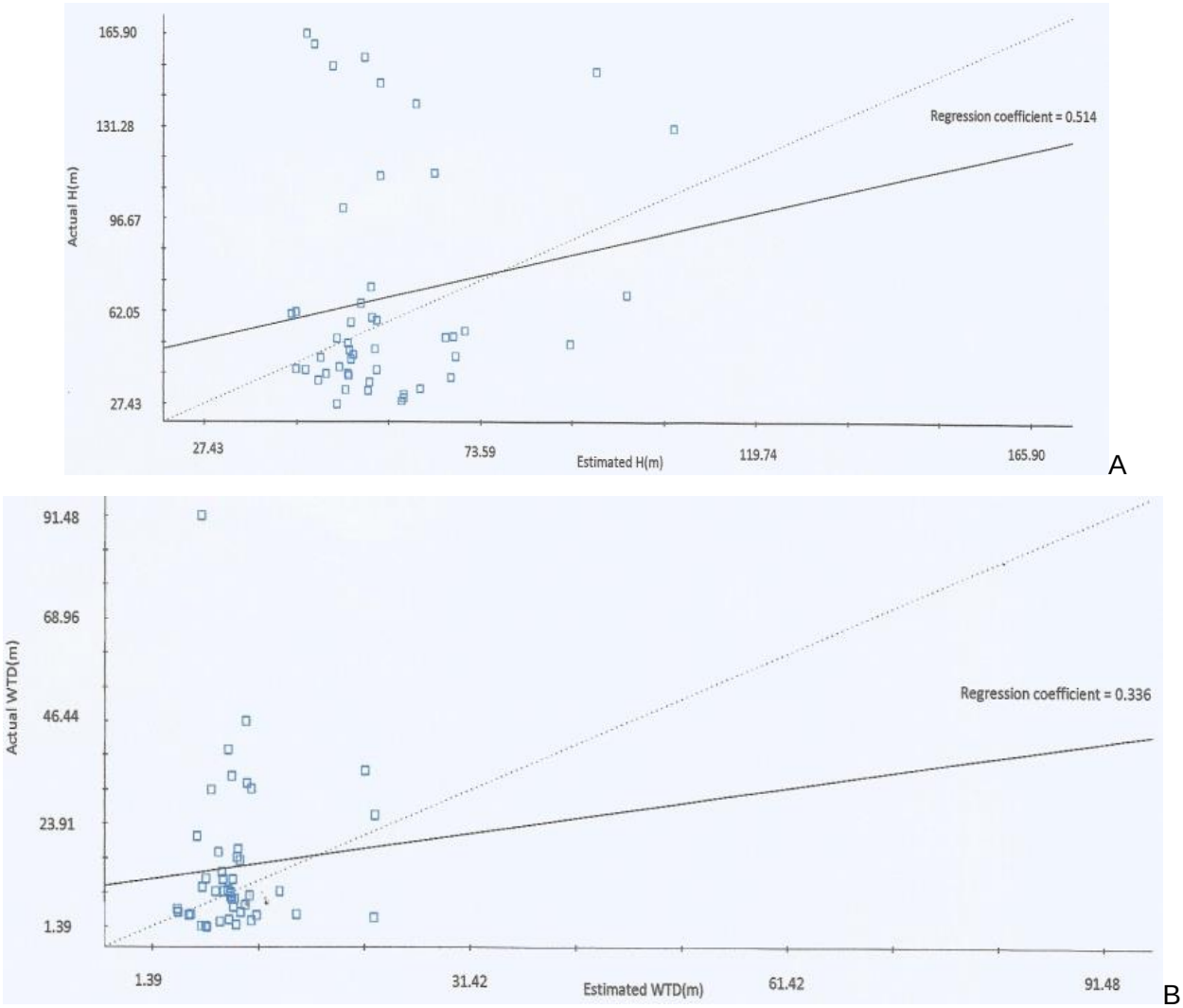

Figure 7. (a) Cross-validation graph of actual vs. estimated values of H(m) data; (b) Cross-validation graph of actual vs. estimated values of WTD(m) data.

the WTD data.

Cross-validation and spatial prediction of H and WTD data

The semivariogram model characteristics shown in Table 3 are used in ordinary kriging to interpolate the groundwater parameters, logH and log(WTD) in the study area. The performance of the kriging-based geostatistical models is optimized by using the leave one out cross validation technique that is usually applied in small datasets (Witten et al., 2011). So, the models in Table 3 are further validated by a process of cross-validation. In the cross-validation procedure, each observed data point, one at a time, (leaving the model otherwise unaltered) is removed and the predicted value is computed at these points. In order to select the most valid model, this process is carried out for each of the three models. Each of the models (Gaussian, Exponential, and Spherical) was fitted, one at a time, on the logH and log(WTD) omnidirectional experimental semivariograms for appraisal. The true and estimated values of the cross-validation are compared using statistical measures. The best model is the one that has the highest regression coefficient (Robertson, 2008), in a cross-validation graph (graph of actual versus estimated values of the groundwater parameters, H and WTD). Regression coefficient represents a measure of the goodness of fit for the least-squares model describing the linear regression equation. A perfect 1:1 fit would have a regression coefficient (slope) of 1. The cross-validation graphs (Figure 7a and b), which compare the actual with the estimated values of H and WTD, respectively, indicate that exponential model with the highest regression coefficient (0.514), revealed in Figure 7a, is the best

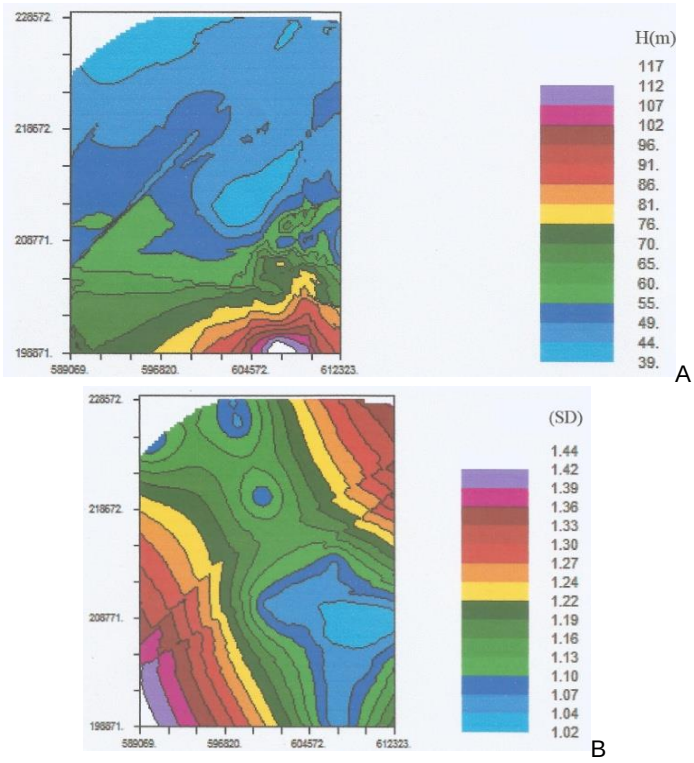

Figure 8. (a) Map of Kriged estimates of aquifer thickness obtained by a back transform of logH to H; (b) Map of Kriged standard deviation (SD) of aquifer thickness.

semivariogram model for the prediction of H data set, while the spherical model, with the highest regression coefficient (0.336), as shown in Figure 7b, is the best semivariogram model for the prediction of WTD data set in the study region.

The general approach that is used for interpolation applies a normalizing transformation followed by ordinary kriging on the transformed variable, and finally the predictions are back-transformed. In the kriging scheme, active lag distance of 12989 and 6500 m for H and WTD parameters, respectively, were specified with a minimum of 30 sample pairs (Istok and Copper, 1988), assured by identifying eight and ten as the minimum and maximum number of neighbors. The kriging system is completed within a round-shaped search neighborhood radius of 18.876 km (approximately half the maximum distance between sample points). The chosen semivariogram models shown in Figure 6a and b and described in Table 3, with the available log H and log(WTD) sample data were used to perform kriged estimation of logH and log(WTD) over the study area. Kriging system also calculates estimation variance or estimation standard deviation.

Mapped values of H and WTD data with estimation variance maps

The kriged logH and log(WTD) maps are used subsequently, to make an estimation of H and WTD values over the study area through a back-transform of logH and log(WTD) to H and WTD. The maps of kriged estimates of H and WTD values which provide an assessment of the H and WTD values over the whole study region, are shown in Figures 8a and 9a, respectively. The estimation standard deviation maps in Figures 8b and 9b, corresponding to H and WTD values, present zones of weak and strong values, and indicate the quality of estimates. The smaller the standard deviation value, the higher the exactness of estimates. Due to border effect and the presence of zones where data points are deficient, highest values of standard deviations of estimates are found towards limits of the study area.

DISCUSSION

The ranges of experimental variograms of logH and log(WTD) are equal to 31.1 and 1.37 km, respectively (Table 3). These distances which indicate the scale of the spatial structure of the variables are significant. It means that two points in the field separated by a distance less than the range remain correlated with each other. For example, the distance 31.1 km, is the maximum distance over which the spatial dependence of the (H) variable

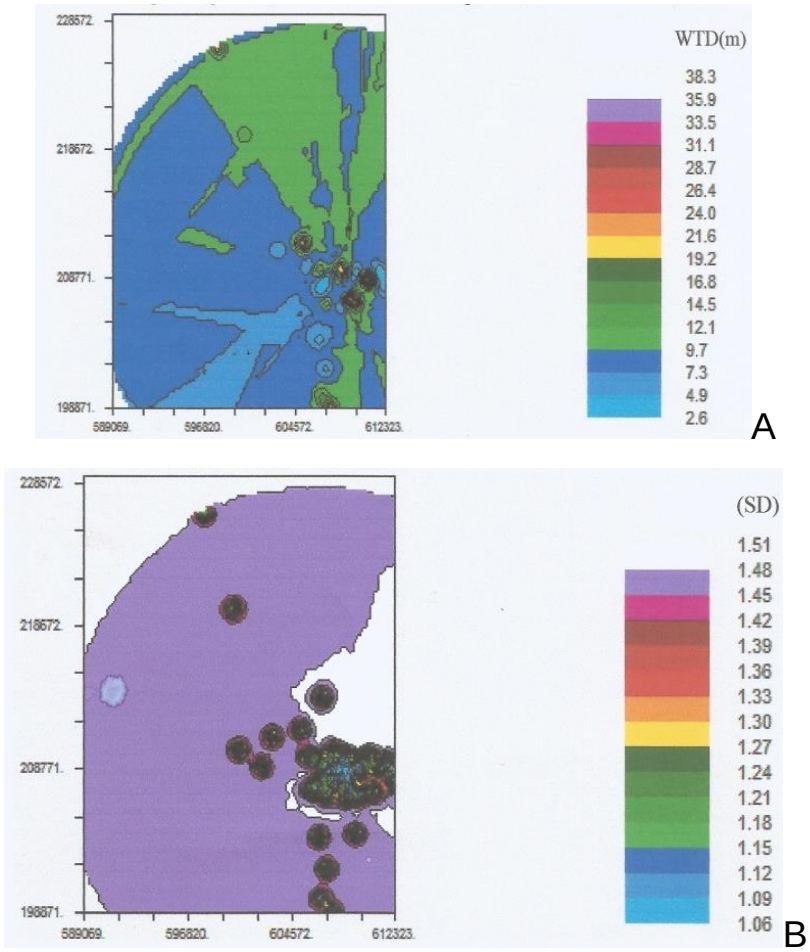

Figure 9. (a) Map of Kriged estimates of water table depth obtained by a back transform of log(WTD) to WTD; (b) Map of Kriged standard deviation (SD) of water table depth.

becomes uncertain, hence, is a measure of the length of influence. The ratio of the nugget variance to the sill represents the importance of this influence (Holawe and Dutter, 1999). These large and small correlation lengths may be explained by patterns of undulation of the terrain in the study region. Of significance in this study is the large nugget effect (measurement error or error at small scale variability), which, in this case, indicates that spatial correlations between individual H and WTD parameters are not strong, but moderate, even at short distances. In practice, the nugget effect is the level of variability at dimensions less than the minimum sample spacing. So, the recognition of the level of nugget effect in association with the spatial range of influence has implications for prospective modelers in the study region. It becomes imperative that the potential modelers gain insight into the scales of spatial variation that might interest them before data collection. This is because variations at micro scales smaller than the sampling distances will appear as part of the nugget value.

According to the generated maps, the southern part of the study area shows relatively higher kriged H-values. That may possibly, be attributed to the existence of Nkporo Formation which is comparatively the higher prolific aquiferous zone. The northern part of the region, underlain by a well compacted, hard Turonian Amasiri Sandstone of the Eze-Aku group is characterized by water scarcity, hence, the presence of relatively lower kriged H-values (Figure 8a). The variation in the distribution of kriged WTD-values in the study region is asymmetrical (Figure 9a). The irregular stretch of kriged WTD-values in the study region may plausibly, be ascribed to the undulating nature of the terrain (Hesse and MacDonald, 1975).

The geostatistical procedure produced satisfactory distribution of high and low values of H and WTD in the study area, similar to available knowledge. In a previous study (Iduma et al., 2016) undertaken in the area, the contour maps (Figures 10a and 11a) of H and WTD, respectively, indicate similar distribution patterns. An

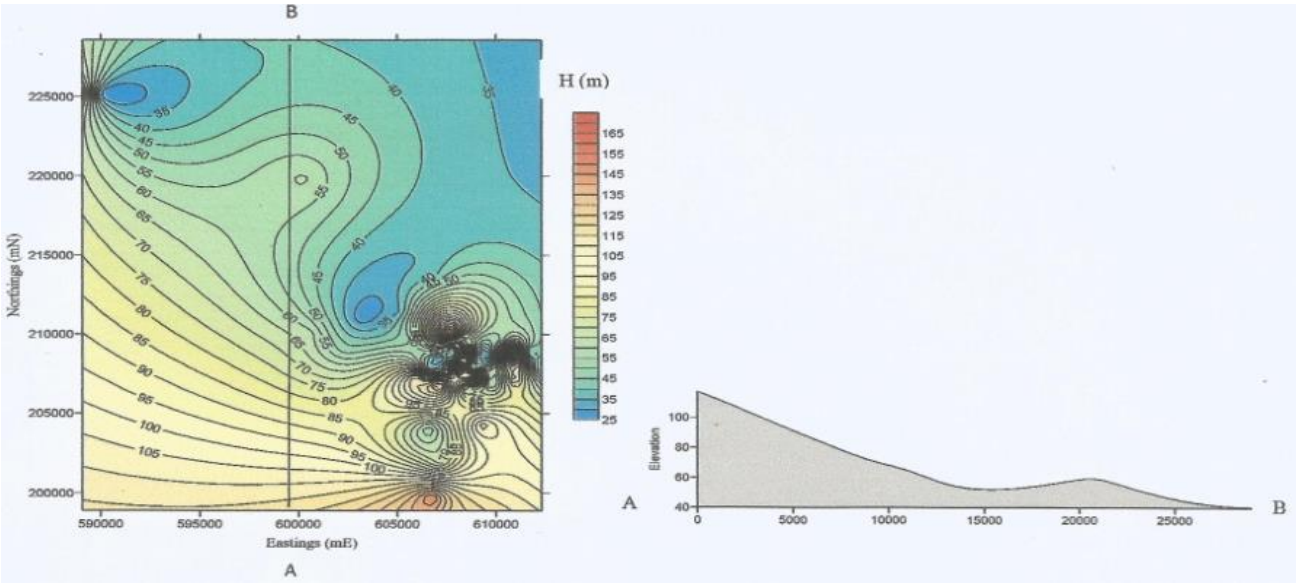

Figure 10. (a) Aquifer thickness-H (m) contour map; (b) Aquifer thickness profile (A-B) (Iduma et al., 2016).

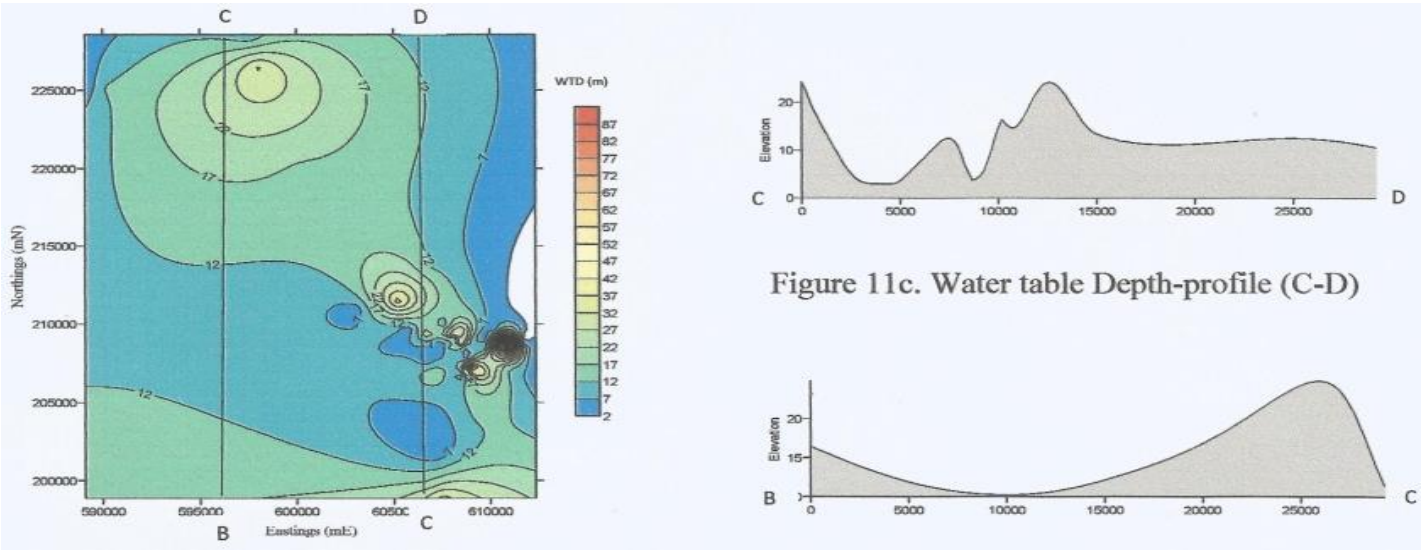

Figure 11. (a) Water table Depth-WTD (m) contour map; (b) Water table Depth-profile (B-C); (c) Watere table Depth-profile (C-D) (Iduma et al., 2016).

isopach map of the aquiferous layer (Figure 10a) shows that aquifer thickness is highly variable, revealing a relatively progressive decrease in values of the aquifer thickness H, in the south-north direction. This condition is confirmed by the longitudinal profile A-B (Figure 10b), which shows a progressive decrease in values of the aquifer thickness H, in the south-north direction. Although the depth to water table tends to be low in some regions, and high in some other parts of the area, generally, the variation in the distribution of the WTD in the study area is irregular as shown in Figure 11a, and illustrated in the longitudinal profiles, BC and CD (Figure 11b and c, respectively).

A comparison of the maps of kriged estimates of H (Figure 8a) and WTD (Figure 9a) with the contour maps (Figures 10a and 11a) from previous study, indicates good agreement in the trend patterns of distribution of these parameter values in the study area. On this basis, the kriged estimates of the H and WTD data-values of the region could be understood to demonstrate coherence, and therefore prove to be reliable. It is pertinent to know that the logarithmic transforms of H and WTD to logH and

log(WTD) are non-linear transforms. So, when the kriged unbiased estimates logH and log(WTD) are back-transformed, their unbiased properties are lost, and the H and WTD values estimated using this procedure are no longer unbiased.

Conclusions

Generally, results of this study showed that ordinary kriging which is best linear unbiased estimator, is the suitable method for estimation of groundwater parameters, H and WTD. By providing the variance of the estimation error, the method gives the quality of the estimation. The variographic analysis of both variables indicates that logH and log (WTD) are stationary variables, characterized by significant nugget effects (discontinuity at the origin of the variogram). Also, it could be concluded that the parameters of the semivariogram used for the structural description, give insight into the spatial pattern of the groundwater parameters, H and WTD. This knowledge has improved the ability to understand the hydrogeology of the study area. Additionally, this study has shown that ordinary kriging constitutes a reliable method to appraise the spatial autocorrelation of groundwater aquifer thickness and water table depth data in interpolation studies. The kriged-H and log(WTD) values are spread over several orders of magnitude, revealing the strong heterogeneity of these parameters in the study region. The generated spatial variability maps of H and WTD will assist water resource managers and policymakers in the development of guidelines in judicious management of groundwater resources for agricultural and drinking purposes in the study area.

CONFLICT OF INTERESTS

The authors have not declared any conflict of interests.

ACKNOWLEDGEMENTS

The authors are deeply indebted to all authors whose works were consulted in the course of this project. They wish to express their appreciation to Mark Baylor, the sales team lead (Gamma Design Software-Plainwell, Michigan-USA) for making it possible to buy the Gamma Design software (15-digit Licence) at student's rate, and later helped to upgrade to 18-digit Licence and Michael Devine (Rockware, Inc. –Colorado USA) who provided the link to Gamma Design Software is also highly admired.

REFERENCES

Ahmadi S, Sedghamiz A (2007). Geostatistical analysis of spatial and temporal variations of groundwater Level. Environ. Monit. *Assess.* 129:277-294.

Andarge YB, Moumtaz R, Tenalem A, Engida Z (2013). Estimating transmissivity using empirical and geostatistical methods in the volcanic aquifers of Upper Awash Basin, central Ethiopia. Environ. Earth Sci. 69(6):1791-1802.

Armstrong M (1989). Review of the applications of geostatistics in the coal industry. Moscow*:* Kluwer Academic Publishers.

Arslan H (2012). Spatial and temporal mapping of groundwater salinity using ordinary kriging and indicator kriging: The case of Bafra Plain Turkey. Agric. Water Manage. 113:57-63.

Arslan H (2013). Application of multivariate statistical techniques in the assessment of groundwater quality in seawater intrusion area in Bafra Plain, Turkey. Environ. Monit. Assess*.* 185(3):2439-2452.

Dash JP, Sarangi A, Singh DK (2010). Spatial variability of groundwater depth and quality parameters in the national capital territory of Delhi. Environ. Manage. 45:640-650.

David M (1977). Geostatistical Ore Reserve Estimation. Amsterdam: Elsevier Scientific Publishing company.

Delbari M (2013). Accounting for exhaustive secondary data into the mapping of water table elevation. Arab J. Geosci. In press.

Deutsch CV, Journel AG (1992). *Geeostatistical Software Library and User's Guide* (2nd edition). New York: Oxford University Press.

Doctor PG, Nelson RW (1981). Geostatistical estimation of parameters for hydrologic transport modeling. Math. Geol. 13:415-428.

Goovaerts P (1997). Geostatistics for natural resources evaluation. New York: Oxford University Press.

Goovaerts P, AvRuskin G, Meliker J, Slotnick M, Jacquez G, Nriagu J (2005). Geostatistical modeling of the spatial variability of arsenic in groundwater of southeast Michigan. Water Resour. Res. 41.

Hesse HW, McDonald RL (1975). The Earth and Its Environment. New York: Dickenson press.

Holawe F, Dutter R (1999). Geostatistical study of precipitation in Austria: time and space. J. Hydrol. 219:70-82.

Iduma REO (2014). Geostatistical modeling of groundwater aquifer in parts of Afikpo and Ohaozara Southeastern Nigeria. (Unpublished Doctoral thesis). Rivers State University of Science and Technology, Port-Harcourt, Nigeria.

Iduma REO, Abam TKS, Uko ED (2016). Dar Zarrouk parameter as a tool for Evaluation of well locations in Afikpo and Ohaozara, Southeasthern Nigeria. J. Water Resour. Prot. 8:501-521.

Isaaks E, Srivastava RM (1989). An introduction to applied geostatistics. New York: Oxford University Press.

Istok JD, Copper RM (1988). Geostatistics applied to Ground Water contamination. Glob. Estimation J. Environ. Eng. 114(9):915-928.

Journel AG, Huijbregts CJ (1978). Minning Geostatistics. London: Academic press.

Kitanidis PK (1997). Introduction to geostatistics: Application to hydrology. Cambridge: University press Cambridge.

Masoomeh D, Masoud BM, Milad K, Meysam A (2013). Investigating spatio-temporal variability of groundwater quality parameters using geostatistics and GIS. Int. Res. J. Appl. Basic Sci. 4(10):3623-3632.

Mehrjardi TR, Jahromi ZM, Mahmodi Sh, Heidari A (2008). Spatial distribution of groundwater quality with geostatistics. World Appl. Sci. J. 4(1):9-17.

Nunes LM, Cunha MCC, Ribeiro L (2004a). Optimal space-time coverage and exploration costs in groundwater monitoring networks. J. Environ. Monit. Assess. 93(1):103-124.

Obiora SC (2002). Evaluation of the Effects of Igneous bodies on the Sedimentary Fills of the Lower Benue Rift and vice versa. (Unpublished PhD thesis). University of Nigeria, Nsukka, Nigeria.

Okereke CO (2012). Sedimentology and facies analysis of Amasiri Sandstone, Lower Benue Trough, South Eastern Nigeria. (Master's thesis). Nnamdi Azikiwe University, Awka, Nigeria.

Okonkwo AC, Okeke PO, Opara AI (2013). Evaluation of Self Potential Anomalies Over Sulphide Ore Deposits at Isiagu, Ebonyi State, Southeastern, Nigeria. Int. Res. J. Geol. Min. 4:9-19.

Pradipika V, Surya DC (2014). Study of spatial variability of ground water depth and quality parameter in haridwar district of uttarakhand. Int. J. Environ. Res. Dev. 4(4):329-336.

Rawat KS, Mishra AK, Sehgal VK, Tripathi VK (2012). Spatial variability of groundwater quality in Mathura District (Uttar Pradesh, India) with

Geostatistical Method. Int. J. Remote Sens. Appl. 2(1):1-9.
Reyment RA (1965). Aspects of Geology of Nigeria. Ibadan: Ibadan University Press.
Robertson GP (2008). GS+: Geostatistics for the environmental sciences (Ver. 10.0). Gamma design software. Plainwell, Michigan, USA.
Simpson A (1954). The Nigerian Coal Fields: The geology of parts of Onitsha, Owerri and Benue Provinces. Geol. Surv. Nig. Bull. 24:1-79.
Simpson A (1955). The Nigerian Coal Fields: The geology of parts of Onitsha, Owerri and Benue Provinces Ball. Geol. Surv. Nig. 24:25-85.
Sophocleous M, Paschetto JE, Olea A (1982). Groundwater network design for Northwest Kansas, using the theory of regionalized variables. Ground Water 20:48-58.
Varouchakis EA, Hristopulos DT, Karatzas GP (2012). Improving kriging of groundwater level data using nonlinear normalizing transformations-a field application. Hydrol. Sci. J. 57:1404-1419.
Webster R, Oliver MA (2001). Geostatistics for environmental scientists. Chichester: Wiley.
Whiteman A (1982). Nigeria: Its Petroleum Geology, Resources and Potential. Graham and Trotham, London.
Witten IH, Frank E, Hall MA (2011). Data Mining: Practical Machine Learning Tools and Techniques: Practical Machine Learning Tools and Techniques. Elsevier, San Francisco.
Yang FG, Cao SY, Liu XN, Yang KJ (2008). Design of groundwater level monitoring network with ordinary kriging. J. Hydrodyn. 20(3):339-346.

academicJournals

Vol. 9(4), pp. 86-95, April 2017
DOI: 10.5897/IJWREE2015.0598
Article Number: D5FDDAC63410
ISSN 2141-6613

http://www.academicjournals.org/IJWREE

International Journal of Water Resources and Environmental Engineering

Full Length Research Paper

Impact of climate change on Lake Chamo Water Balance, Ethiopia

Elias Gebeyehu

Department of Hydraulic and Water Resources Engineering, Arba Minch Institute of Technology, Arba Minch University, P.O. Box 021, Ethiopia.

Received 8 July, 2015; Accepted 4 January, 2016

One of the most significant potential concerns of climate change is to understand changes in hydrological components and subsequent change in lakes water balance. In view of this study, the water balance components such as surface water inflow from gauged and ungauged sub-watersheds, precipitation and evaporation pattern of the natural reservoir and their associated impacts vis-à-vis altering the water balance of terminal Lake Chamo has a major concern in the present study. The raw A1B scenario outputs are characterized by significant biases and hence subjected to bias correction before applying in the hydrological modeling. The bias correction for A1B scenario for precipitation, maximum and minimum temperature was done by using linear scaling approach. This analysis is based on projection of two different scenarios of future time horizons: 2030s (2031-2040) and 2090s (2091-2100). A hydrological model, Hydrological Byråns Vattenbalansavdelning (HBV), was used to simulate the current and future inflow to the lake. The performance of the model was assessed through calibration and validation process and resulted in R^2 from 0.64 to 0.81 during calibration and from 0.63 to 0.77 during validation and the relative volume error RV_E is from -1.77 to 4.42% at the three stations. Mean annual inflow to Lake Chamo from gauged and un-gauged catchment is 257 $mmyr^{-1}$. The estimated runoff for the period 2030s and 2090s is 215 and 147$mmyr^{-1}$ respectively. The result shows that the mean annual inflow is decreased by 16.3 and 42.8% in 2030s and 2090s, respectively from the base time period. The result revealed the maximum and minimum temperatures increase for the two scenarios in future time horizons. However, precipitation decreased in all future time horizons. The A1B scenario reveals the decreasing pattern of lake water storage due to decrease of inflows components such over lake precipitation and surface water inflow in all the future time horizons. In this scenario, the over-lake evaporation is increased by 0.73 and 2.6% at 2030s and 2090s.

Key words: Water balance, Lake Chamo, RCM, A1B, climate variability, HBV model.

INTRODUCTION

The impact of climate change on water resources is becoming a hotspot across the globe over the last couple of decades. Climate change wil likely alter the hydrological cycle in many ways and it may cause substantial impacts on water resource availability and changes in water quality.

E-mail: eliasg2000@gmail.com.

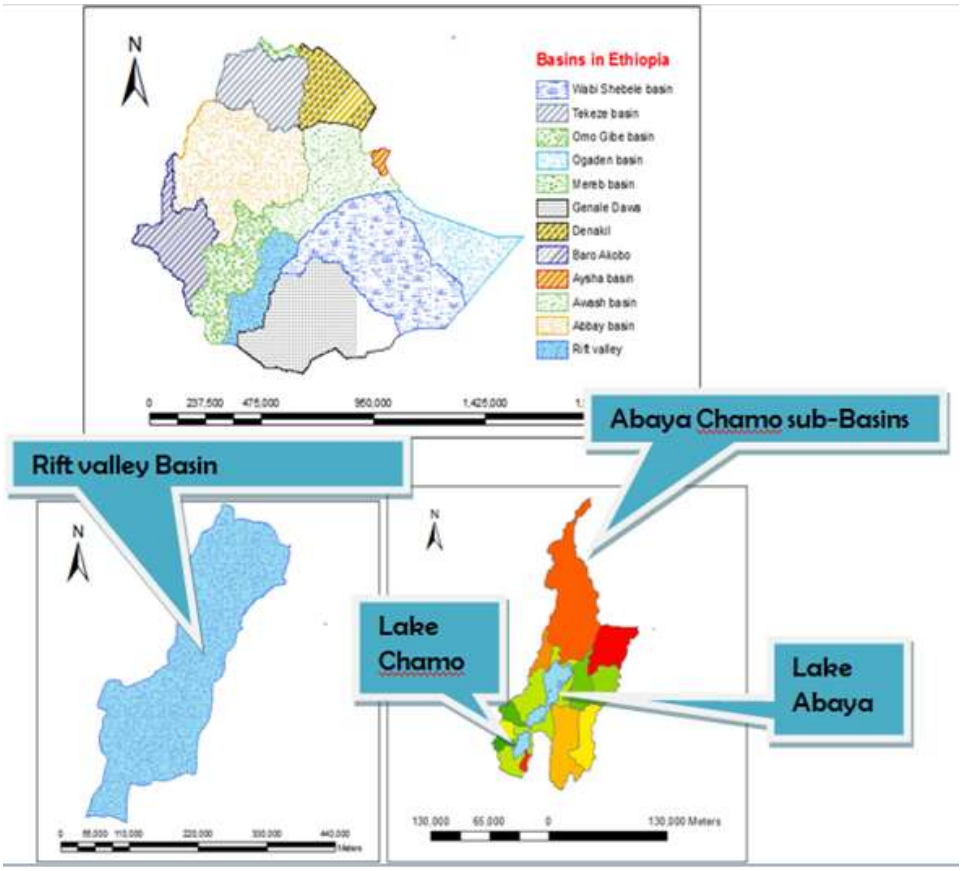

Figure 1. Map of the study area.

Lake is a large, inland body of standing water that occupies a depression in the land surface. Lakes and lake shores are attractive places to live and for recreation. Clean, sparking water, abundant wildlife, beautiful scenery, aquatic recreation and fresh breezes all come to our mind when we think of going to the lake. Despite the great value, lakes are delicate and ephemeral.

The main objective of this study was to identify and investigate the possible future climate change effects on Lake Chamo water balance. The results will be used to forecast lake water balance fluctuation and to suggest mitigation measures to alleviate the ensuing problems.

Study area

The southern part of Ethiopian Rift valley system is characterized by two adjoining lakes, Lake Abaya and Lake Chamo, separated by a small naturally created ridge called “God’s Bridge” from the Abaya-Chamo Sub basin. Geographic Abaya Chamo sub-basin extends from 4°37’13” to 6°59’52” N latitude and 36°14’47” to 40°05’47” E longitude.

Lake Chamo is located in Southern Nations, Nationalities and People’s Republic (SNNPR). It is part of the main Ethiopian rift system, situated to the south of Lake Abaya and the town of Arba Minch with mean elevation of with 1108 m (Figure 1).

WATER BALANCE TERMS FROM OBSERVED DATA

In this study, the Lake Chamo water balance (Equation 1) is solved for the period 1995 – 2004. Observation time series are available for rainfall (five stations), evaporation (two stations) and runoff from gauged catchments (one catchment). For both rainfall and evaporation area, averaged estimates are made by simple interpolation while, after screening, runoff time series are directly used.

$$\frac{\Delta S}{\Delta t} = P + Q_{gauged} + Q_{ungauged} - E - Q_{out}$$

Where: $\frac{\Delta S}{\Delta t}$: Is the change in storage over time [Mm^3 /day]; $\mathbf{P}$: the lake’s areal rainfall of past records and RCM scenario outputs [Mm^3 /day]; $\mathbf{E}$: the open water evaporation of past records and RCM scenario outputs [Mm^3 /day]; $\mathbf{Q_{gauged}}$: the gauged catchments inflow estimated by HBV based on past records and RCM scenario outputs [Mm^3 /day]; $\mathbf{Q_{ungauged}}$: the ungauged catchments inflow

estimated by HBV based on past records and RCM scenario outputs [Mm^3 /day]; $\mathbf{Q_{out}}$: the outflow from lake [Mm^3/day].

Meteorological balance terms

Daily lake rainfall has been estimated through inverse distance squared interpolation, inverse distance linear interpolation and through Thiessen polygons. Data for the period 1991– 2000 from Arba Minch, Mirab Abaya, Chencha, Gerese and gato station are used for the interpolation.

To estimate lake evaporation, the Penman-combination equation (Maidment, 1993) is selected, which has wide application as a standard method in hydrologic engineering. In this equation, the energy balance is combined with a water vapour transfer method and results in an equation to compute the evaporation from open water surface using standard climatological records of daily sunshine hours, temperature, humidity and wind speed. The Penman-combination equation for open water evaporation is:

$$\mathbf{ET_0} = \frac{0.408\Delta(R_n - G) + \gamma\frac{900}{T+273}U_2(e_s - e_a)}{\Delta + \gamma(1 + 0.34U_2)}$$

Where: ETo- Reference evapotranspiration [mm day^{-1}]; R_n- net radiation at the crop surface [MJ m^{-2} day^{-1}]; G- soil heat flux density [MJ m^{-2} day^{-1}]; T- mean daily air temperature at 2 m height [°C]; U_2- wind speed at 2 m height [m s^{-1}]; e_s- saturation vapour pressure [kPa]; e_a- actual vapour pressure [kPa]; Δ- slope vapour pressure curve [kPa $°C^{-1}$]; γ - psychrometric constant [kPa $°C^{-1}$].

RUNOFF FROM UNGAUGED CATCHMENTS

Runoff from ungauged catchments is estimated by three procedures that are of different complexity. The first procedure applies a regionalization procedure where a regional model (Merz and Bloschl, 2004: Booij et al., 2007) is established between catchment characteristics and model parameters that in turn are used for ungauged catchment modeling. A second procedure simply transfers model parameters from neighboring or nearby catchments to ungauged catchments to allow for runoff simulation. In the third procedure, parameter sets of gauged catchments are transferred to ungauged catchments by simple comparison of catchment size. In all three procedures, the HBV-IHMS model (Integrated Hydrological Modeling System) (IHMS, 2006) is selected for simulation of catchment runoff. Effectiveness of the HBV model approach in regionalization studies is reported by Seibert (1999), Booij (2005) and Booij et al. (2007). Our study is different from these works in the sense that we simply applied regionalization procedures to seek closure of Lake Tana water balance while much work in regionalization and ungauged catchment hydrology focus on assessing predictive capability of runoff models as advocated by the International Association of Hydrologic Sciences (IAHS) in their 10-year Prediction in Ungauged Basins (PUB) project (Sivapalan et al., 2003). Such approaches also aim at assessing effectiveness of preference and non preference based multi-objective calibration (Wagener and Wheater, 2004) and also aims at testing specific catchment characteristics in establishing a regional model. Also, most studies use a large number of catchments (Booij et al., 2007) from which a large number is assumed to be ungauged to serve calibration and validation purposes while we only use five gauged catchments and a selection of catchments characteristics that are available from simple soil, land use and geologic maps or that can be extracted from a satellite-based SRTM DEM of 90 m resolution.

HBV-IHMS

The Hydrological Byråns Vattenbalansavdelning (HBV) model is a conceptual rainfall-runoff model for continuous simulation of catchment runoff. The model consists of subroutines for precipitation and snow accumulation, soil moisture accounting, actual evaporation and uses simple transformation functions and routing procedures. Soil moisture accounting is governed by two simple relations that are parameterized by FC which is the maximum soil moisture storage (mm) in the model, LP which is a limit for potential evapotranspiration and parameter which controls the contribution of soil moisture storage (SM) to the response function $\Delta Q/\Delta P$.

$$\frac{\Delta Q}{\Delta P} = \left[\frac{SM}{FC}\right]^{Beta}$$

Q denotes discharge and P denotes precipitation while $\Delta Q/\Delta P$ is to be interpreted as a runoff coefficient. Actual evapotranspiration, Ea, which is controlled by a soil moisture routine is linearly related to the potential evapotranspiration, Ep, and is:

$$\mathbf{EA} = \mathbf{Ep}\left[\frac{\mathbf{SM}}{\mathbf{LP} * \mathbf{FC}}, \mathbf{1}\right]$$

In HBV-IHMS, the runoff routine comprises two reservoirs that distribute generated runoff over time to obtain the quick and slow parts of a catchment runoff hydrograph. Runoff generated from the upper reservoir represents quick runoff discharges while runoff from the lower reservoir represents groundwater discharges.

$$\mathbf{Q_o} = \mathbf{K} * \mathbf{UZ}^{(1+\mathbf{Alfa})}$$

$$\mathbf{Q_1} = \mathbf{K4} * \mathbf{LZ}$$

Where: $\mathbf{Q_o}$: Direct runoff from upper reservoir (mm), **K**: recession coefficient upper reservoir, **UZ**: upper reservoir storage (mm), $\mathbf{Q_1}$: lower reservoir outflow (mm), **LZ**: lower reservoir storage (mm) and **K4**: recession coefficient lower reservoir storage.

Model performance

The performance of the model must be evaluated for the extent of its accuracy. Hence, for this study, the model performance in simulating observed discharge was evaluated during calibration and validation by; inspecting simulated and observed runoff graphs visually, by calculating Nash and Sutcliffe efficiency criteria R^2 (commonly used in hydrological modeling) and by calculating the Relative Volume Error (RV_E).

The Nash and Sutcliffe coefficient (R^2) is a measure of efficiency that relates the goodness-of-fit of the model to the variance of measured data. R^2 can range from - ∞ to 1 and an efficiency of 1 indicates a perfect match between observed and simulated discharges. R^2 value between 0.9 and 1 indicate that the model

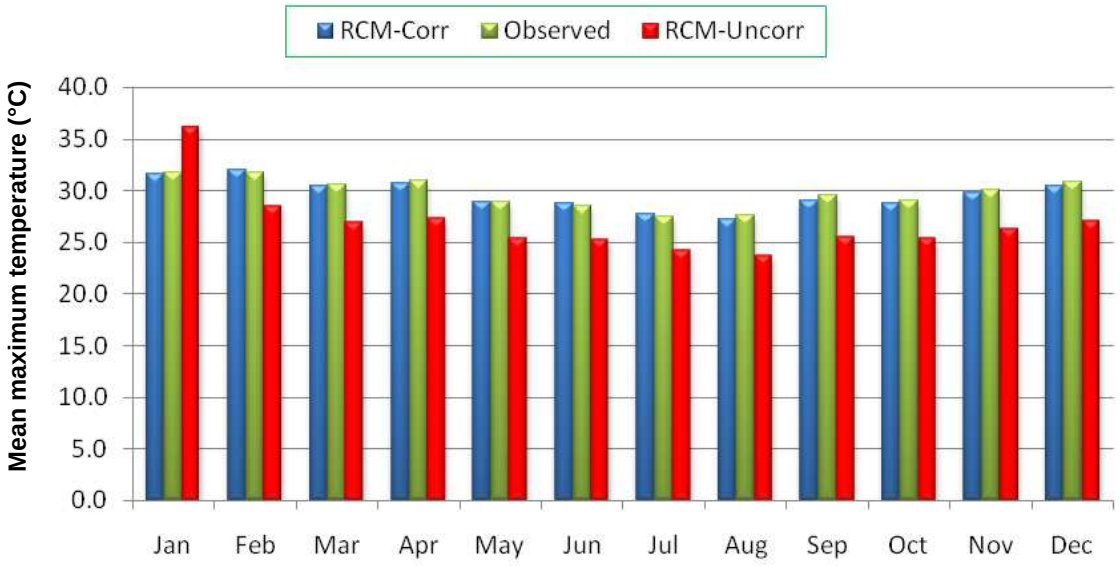

Figure 2. Comparison of mean monthly maximum temperature at Arba Minch Station.

performs very well while values between 0.6 and 0.8 indicate the model performs well (Rientjes et al., 2011). The largest disadvantage of this efficiency criterion is that larger value in a time series are strongly overestimated where as lower values are of minor importance. For the quantification of runoff prediction, this leads to an overestimation of model performance during peak flows and underestimation during low flow conditions:

$$\mathbf{R^2 = 1 - \frac{\sum_{i=1}^{n}\left(Q_{sim(i)} - Q_{obs(i)}\right)^2}{\sum_{i=1}^{n}\left(Q_{sim(i)} - \bar{Q}_{obs(i)}\right)^2}}$$

Where,

$\mathbf{Q_{obs}}$: Observed flow, $\mathbf{Q_{sim}}$: simulated flow and $\mathbf{\bar{Q}_{obs}}$: Average of observed flow.

The $\mathbf{RV_E}$ can vary between ∞ and - ∞ but it performs best when a value of 0 (zero) is generated. Since an accumulated difference between simulated, $\mathbf{Q_{sim(i)}}$ and $\mathbf{Q_{obs(i)}}$ is observed, discharge is zero. A relative volume error between +5% or -5% indicates that a model performs well while relative volume errors between +5 and +10 and -5 and -10% indicates a model with reasonable performance (Rientjes et al., 2011).

$$\mathbf{RV_E = \left[\frac{\sum_{i=1}^{n} Q_{obs(i)} - \sum_{i=1}^{n} Q_{sim(i)}}{\sum_{i=1}^{n} Q_{obs(i)}}\right] * 100\%}$$

RESULTS AND DISCUSSION

Maximum temperature

Observed, uncorrected RCM (RCM-uncorr) and bias corrected (RCM-corr) mean monthly maximum and minimum temperature magnitudes are presented for Arba Minch stations (Figures 2 and 4). RCM bias correction is done for A1B scenario minimum and maximum temperature, which shows significant difference from bias uncorrected mean monthly when compared with mean monthly-observed data. The deviation of maximum and minimum temperature between corrected and uncorrected RCM is 3.5 to 4.6°C and 0.1 to 1.6°C at Arba Minch station. This result indicates that using the RCM output without doing bias correction may lead to enormous uncertainty of hydrological analysis.

The maximum and minimum monthly absolute model error is found in the month of September and May, respectively. On average, the monthly absolute model error is found to be 0.1°C (Figure 3).

Minimum temperature

Bias corrected minimum temperature also shows a reasonably good agreement with the observed minimum temperature for all the months.

The maximum and minimum monthly absolute model error is found in the month of April and March, respectively. On average, the monthly absolute model error is found to be 0.2°C (Figure 5).

Precipitation

In comparison with the minimum and maximum temperature, the precipitation could not be able to replicate the historical (observed) data. This is due to

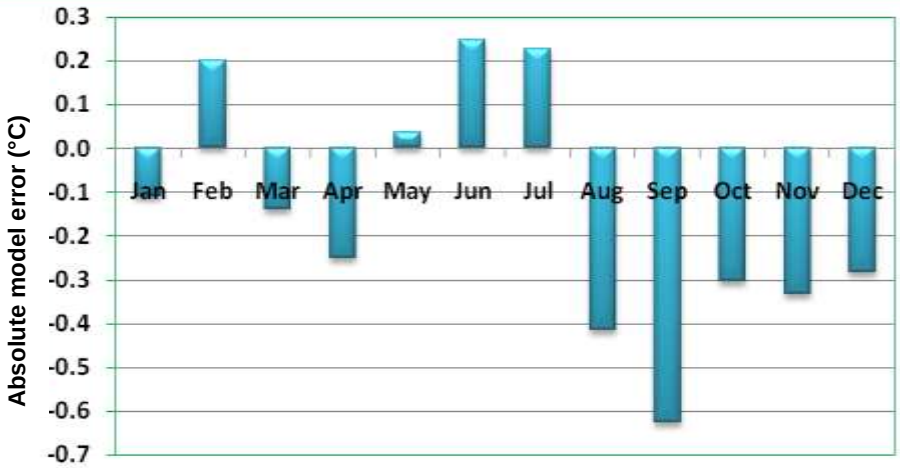

Figure 3. Absolute model error of maximum temperature (1991-2000).

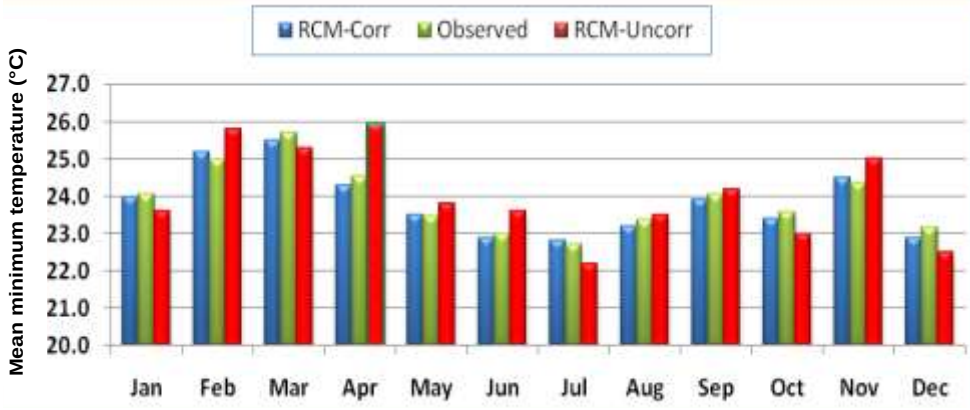

Figure 4. Comparison of mean monthly minimum temperature at Arba Minch station.

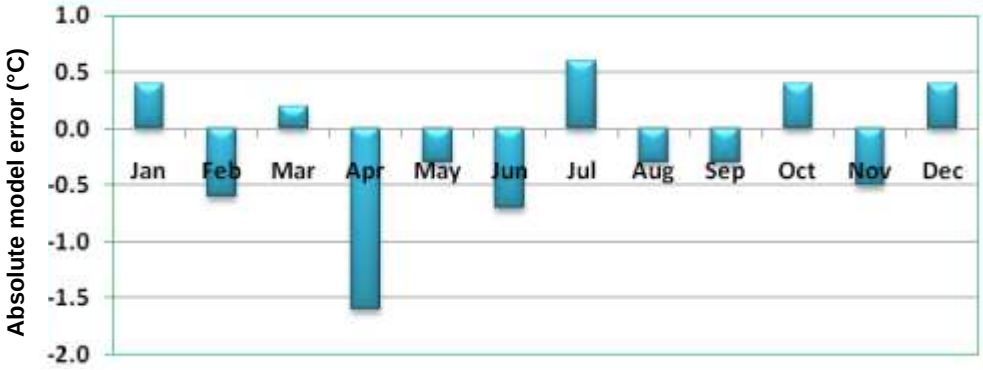

Figure 5. Absolute model error of minimum temperature (1991-2000).

complicated nature of precipitation processes and its distribution in space and time. Climate model simulation of precipitation has improved over time but is still problematic; also rainfall predictions have a larger degree of uncertainty than those for temperature. This is because rainfall is highly variable in space and so the

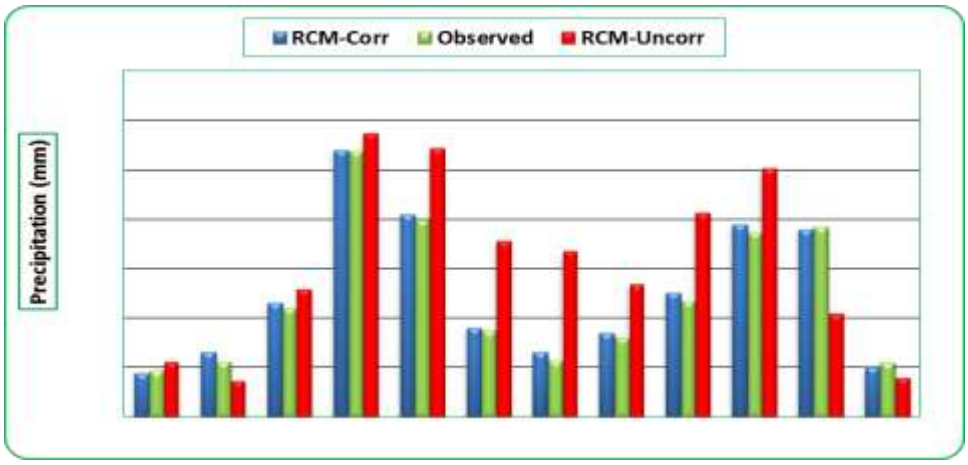

Figure 6. Mean monthly precipitation (1991-2000).

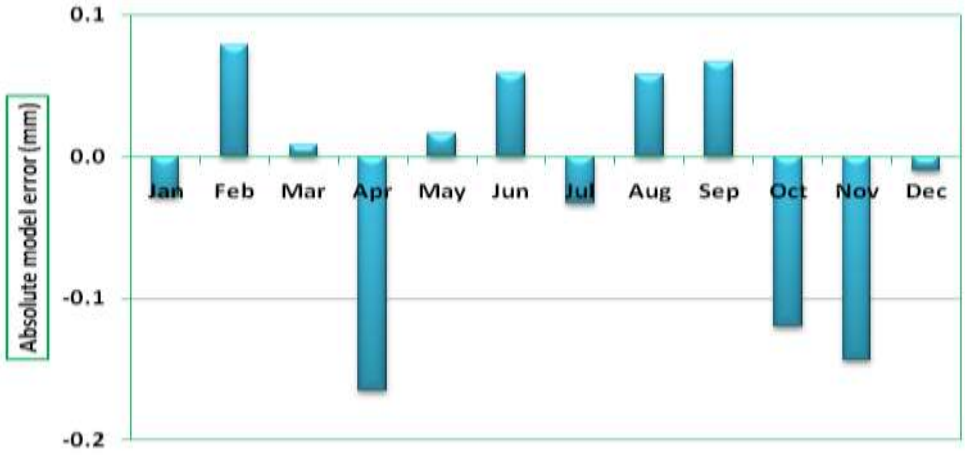

Figure 7. Absolute model error of precipitation (1991-2000).

relatively coarse spatial resolution of the current generation of climate models is not adequate to fully capture that change.

The bias corrected precipitation shows an average absolute model error of 0.1 mm (Figure 7).

Projected future climate change (scenario generation)

The term anomaly means a deviation of future climate condition from a baseline period (1991-2000) climate condition. In this study baseline period climatic condition is analyzed based on historical observations of the study area under consideration the anomaly of monthly precipitation is calculated as the difference from future monthly average precipitation to the baseline period monthly average precipitation values. Positive anomaly indicates increase from the baseline period value; a negative anomaly indicates decrease from the baseline period value. The temperature is also calculated in the same way precipitation is calculated.

RCM model scenarios (A1B) were also analyzed to generate temperature and precipitation scenarios of the two future time windows, namely 2031-2040(2030s) and 2091-2100(2090s).

Projected changes in monthly rainfall statistics

Projected changes in monthly rainfall statistics are vital means of evaluating the characteristics of rainfall at the study site. Figure 6 shows the general pattern of the change anomalies in April monthly mean precipitation for future period at Arba Minch station.

The RCM A1B scenario show an overall decreasing pattern in the month of January–April (0.2-1.8 mm) and October to December (0.4-2.4 mm) at 2030s and January to February (0.8-0.9 mm), April (0.9 mm) and October to December (0.6-3.0 mm) at 2090s. The consistent

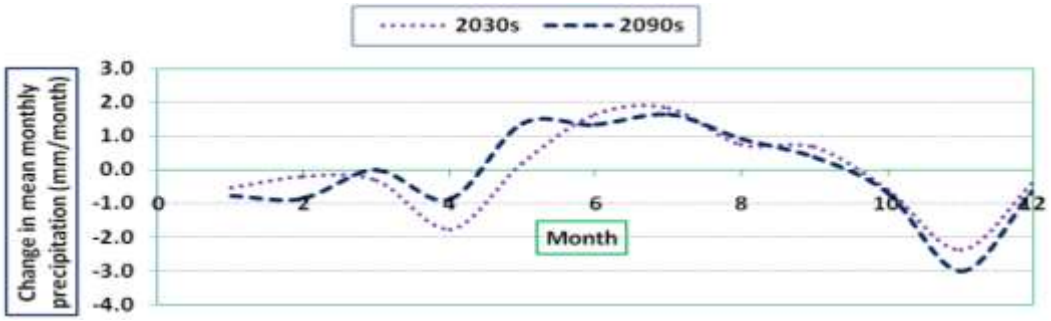

Figure 8. Change anomalies of mean precipitation for future windows at Arba Minch station.

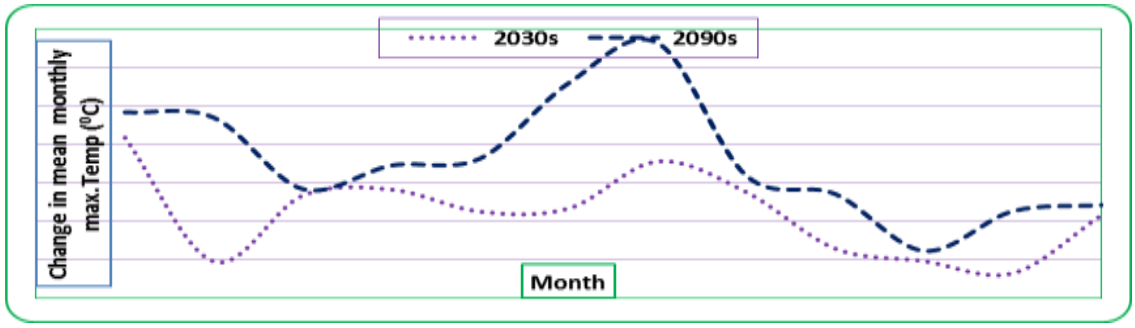

Figure 9. Change anomalies of monthly mean maximum temperature for future windows at Arba Minch station.

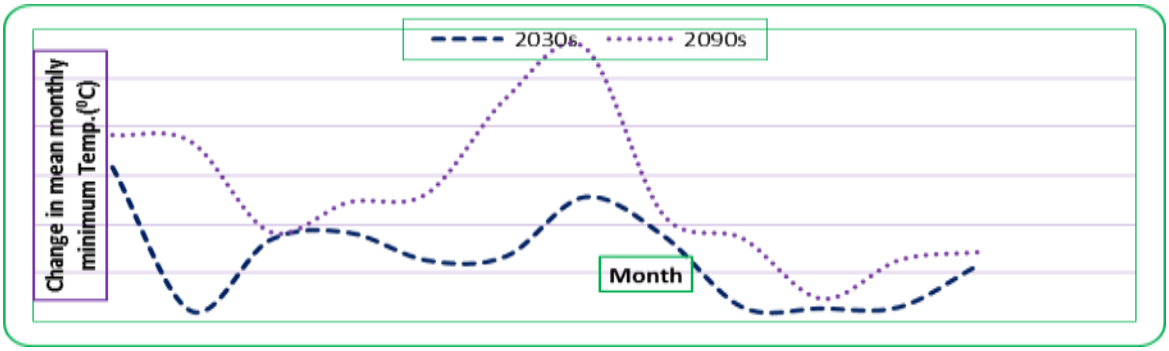

Figure 10. Change anomalies of monthly mean minimum temperature for future windows at Arba Minch station.

increasing pattern is revealed in the month of May to September (0.2-1.8 mm) at 2030s and 0.4-1.6 mm at 2090s. The month March at 2090s showed a similar pattern with the baseline period. The percentage change of future precipitation against observed baseline period is decreased by 3.9% at 2030s and 4.2% at 2090s (Figure 8).

Projected changes in monthly maximum temperature statistics

Figure 9 shows the change anomalies in mean monthly maximum temperature for future periods. The simulation indicates an overall decreasing pattern in the month November, February and October by 0.2°C and increasing pattern in the rest months from +0.1 to +1.6°C at 2030s. At 2090s, simulation indicates an overall increasing pattern of +0.1 to +2.8°C. The percentage change of maximum temperature against observed baseline period is increased by 2.04% at 2030s and 4.4% at 2090s.

Projected changes in monthly minimum temperature statistics

Figure 10 shows the change anomalies in mean monthly minimum temperature of for future periods. The future scenario simulation indicates an overall increasing pattern

Table 1. Optimum parameter during the calibration

S/N	Catchment	Parameter									
		Alfa	Beta	Fc (mm)	hq	K4	Khq	lp	Maxbas (day)	Perc (mm/day)	Rfcf
1	Kulfo	0.6	1	1500	21.42	0.008	0.06	1	1	3.5	1.54
2	Sile	4.8	0.5	1500	35	0.03	0.02	1	1	0.7	1.19
3	Sago	4.8	0.6	1500	32	0.02	0.02	1	1	0.6	1.18

of +0.1 to +1.6°C at 2030s and +0.2 to +2.8°C at 2090s. The percentage change of future temperature against observed baseline period is increased by 2.07% at 2030s and 5.5% at 2090s.

Evaluating the performance of RCM simulations against observed baseline period

Downscaling is conducted for precipitation, maximum and minimum temperature based on data of Arba Minch, Mirab Abaya, Gato and Konso stations for the period of 1991-2000. RCM (A1B scenario) model output performance is evaluated based on comparison of historic (observed) baseline period, 1991-2000. Daily mean downscaled RCM output and observed precipitation, maximum and minimum temperature is compared to check whether the historic (observed) condition can be replicated or not. Therefore, it is vital that model simulated precipitation and temperature data should have the same statistical properties as the observed meteorological time series data.

Hydrological model

Calibration and validation

The HBV-model is calibrated and validate for the observed period of ten years (1995-2004) and the best-fit parameters sets are selected. Calibration aimed at the water balance and over all shape agreement of the observed discharge using RV_E (relative volume error) and R^2 (Nash and Sutcliffe coefficient). In simulation of the runoff, the observed period is divided into three zones, namely; warm up period (1995), calibration period (1996-2001) and validation period (2002-2004).The calibration and validation is carried out for both daily and monthly time steps. It is observed that the model has a very good capability to simulate the observed flow for both low flow and high flow period.

Table 1 shows recommended values of selected parameters for Chamo sub-basin to be calibrated and the most optimum parameter set used in the calibration.

The observed and simulated runoff hydrograph using the above optimum parameter is shown in Figure 11. Visual inspection of the observed and simulated runoff shows good performance of the model.

Generally, the values of the performance criteria show that during the calibration period, overall performance of HBV model is somewhat better as compared to the validation period (Table 2).

Water balance

There are many processes that contribute to the Lake Chamo water balance. Inflow to the Lake Chamo is the sum of lake areal rainfall, runoff from gauged and un-gauged catchments. The outflow component of the Lake Chamo is open water evaporation. The groundwater flow component is assumed to be negligible and hence not included in the present analysis. Lake level is simulated by using area-volume and elevation-volume relationships.

After estimation of the lake water balance components, a spreadsheet water balance model is developed. The model is developed to calculate the inflow and outflow components separately in terms of volume. The initial volume and area of the lake is simply defined by fixing the initial value to an observed lake level. In the model, both evaporation and rainfall are defined as a function of the lake surface area (Table 3).

In general, result of A1B scenario indicates a decrease of inflows to the lake and over lake precipitation, but an increase of over lake evaporation for the future. The decrease of lake water balance for the future indicates the lake water drop off.

There are still many sources of uncertainty and errors in the water balance but quantifying and reducing the errors is far from trivial. Uncertainties associated with lake-groundwater interaction estimations of lake water balance components such as open water evaporation, lake areal rainfall, runoff from gauged and un-gauged catchments may affect the lake water balance modeling endeavor (Table 3).

Daily lake water level simulation

For lake level simulation all mass balance terms are solved on a daily step and results of lake level simulations are compared with the observed lake levels (Figure 12).

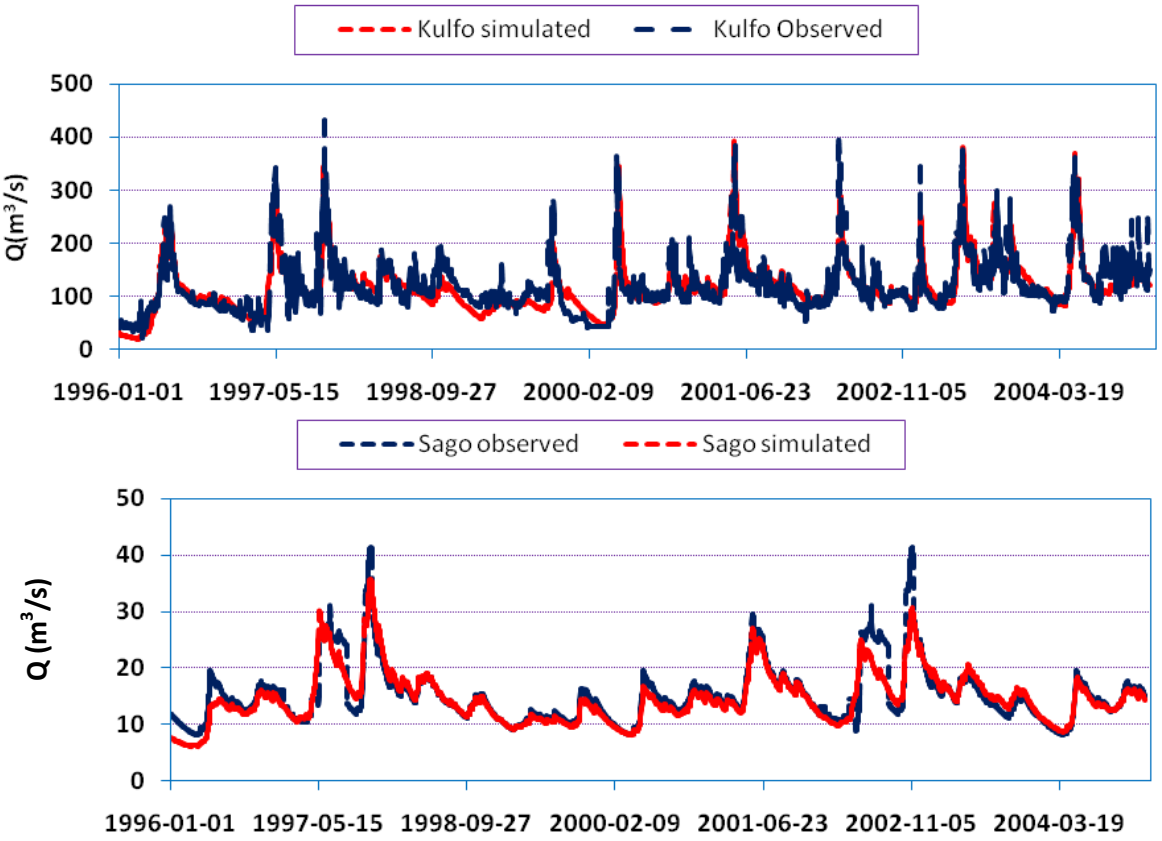

Figure 11. Observed and simulated graph of Kulfo and Sago catchment.

Table 2. Summarized objective function during calibration and validation.

Catchment name	Calibration		Validation	
	R^2	RV_E	R^2	RV_E
Kulfo	0.64	0.85	0.63	1.26
Sago	0.79	4.42	0.77	2.25
Sile	0.81	2.13	0.76	-1.77

Table 3. Lake Chamo water balance components.

Water balance components	Unit	1996-2004	2030s	2090s
Lake areal rainfall	$mmyr^{-1}$	897	869	808
	$MCMyr^{-1}$	295	286	265
Gauged river inflow	$mmyr^{-1}$	161	153	98
	$MCMyr^{-1}$	53	50	32
Un-gauged river inflow	$mmyr^{-1}$	96	62	49
	$MCMyr^{-1}$	32	20	16
Lake evaporation	$mmyr^{-1}$	1217	1226	1249
	$MCMyr^{-1}$	400	403	410
Lake outflow		0	0	0

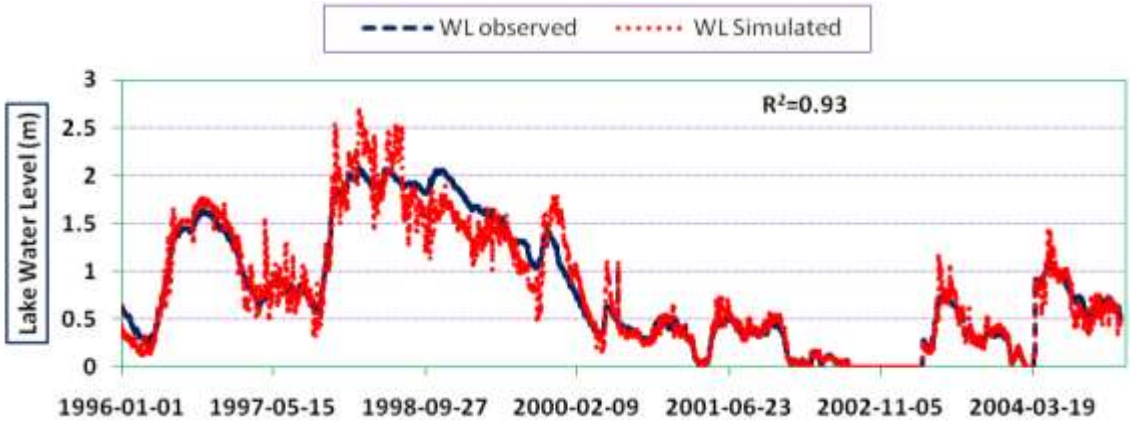

Figure 12. Observed and simulated graph of Lake Chamo water level.

Conclusion

In this study, daily water balance of Lake Chamo was simulated giving due emphasis for un-gauged river inflows. River flow from un-gauged catchment is estimated by transferring model parameters of gauged catchments by area ration approach. Based on the study conducted, the following conclusions were drawn.

1. The result of climate projection reveals that the RCM bias corrected by linear scaling approach has very good ability to replicate the historical maximum and minimum temperature and precipitation for the observed period.
2. The percentage change of maximum temperature scenario against observed baseline period is increased by 2.04% at 2030s and 4.4% at 2090s. The percentage change of minimum temperature scenario against observed baseline period is increased by 2.07% at 2030s and 5.5% at 2090s. This causes its own impact on the lake water balance by increasing the evaporation from the lake.
3. The result shows the mean annual precipitation is decreased by 3.1 and 10% in 2030s and 2090s, respectively from the base time period. This causes its own impact on the Lake water balance by changing the volume.
4. HBV-96 hydrological model is used for calibration and validation by using daily data of precipitation and potential evapo-transpiration. The result of hydrological model calibration and validation indicates that the HBV model simulates the runoff considerably good for the study area. The model performance criterion which is used to evaluate the model result indicates that the daily Nash and Sutcliffe efficiency criteria (R^2) was between 0.81 and 0.64 during calibration and 0.77 and 0.63 during validation period.
5. The simulated flow at 2030s and 2090s with scenario from RCM A1B shows reduction of runoff in the watersheds and it is directly related to the reduction in precipitation and rising in potential Evapo-transpiration. The mean annual inflow is decreased by 16.3 and 42.8% in 2030s and 2090s respectively from the base time period. 6.32.1% of inflow of Lake Chamo is from ungauged river and 67.9% is from gauged river.
7. Human activity and catchment mismanagement have accelerated lake water degradation.

CONFLICT OF INTERESTS

The authors have not declared any conflict of interests.

REFERENCES

Booij MJ (2005). Impact of climate change on river flooding assessed with different spatial model resolutions. J. Hydrol. 303(1-4):176-198.
Booij MJ, Rientjes THM, Deckers DLEH, Krol MS (2007). Regionalisation for runcertainity eduction in flows in ungauged basins. In: Quantification and reduction of predictive uncertainty for sustainable water resources management: proceedings of symposium HS2004 at IUGG2007, Perugia, 7-13 July 2007. ed. by Boegh E...[et.al] Wallingford : IAHS, 2007. ISBN 978-19015078-09-1 (IAHS Publication) 313:329-337.
Maidment DR (1993). Handbook of Hydrology, McGraw-Hill. https://books.google.com.ng/books/about/Handbook_of_hydrology.html?id=4_9OAAAAMAAJ&redir_esc=y
Merz R, Blöschl G (2004). Regionalisation of catchment model parameters. J. Hydrol. 287(1-4):95-123.
Rientjes THM, Perera JBU, Haile AT, Gieske ASM (2011). Hydrological balance of Lake Tana, upper Blue Nile basin, Ethiopia. In: Nile River Basin: Hydrology, Climate and Water Use: e-book
Seibert J (1999). Regionalisation of parameters for a conceptual rainfall-runoff model. Agric. Forest Meteorol. 98-99:279-293.
Sivapalan M, Takeuchi K, Franks SW, Gupta VK, Karambiri H, Lakshmi V, Liang X, McDonnell JJ, Mendiondo EM, O'connell PE, Oki T, Pomeroy JW, Schertzer D, Uhlenbrook S, Zehe E (2003). IAHS Decade on Predictions in Ungauged Basins (PUB), 2003-2012: Shaping an excuting future for the hydrological sciences. Hydrol. Sci. J. Sci. Hydrol. 48(6):857-880.
Wagener T, Wheater HS, Gupta HV (2004). Rainfall-Runoff modelling in gauged and ungauged catchment, Imperical College Press.

International Journal of Water Resources and Environmental Engineering

Related Journals Published by Academic Journals

- *International Journal of Computer Engineering Research*
- *Journal of Chemical Engineering and Materials Science*
- *Journal of Civil Engineering and Construction Technology*
- *Journal of Electrical and Electronics Engineering Research*
- *Journal of Engineering and Computer Innovations*
- *Journal of Engineering and Technology Research*
- *Journal of Mechanical Engineering Research*
- *Journal of Petroleum and Gas Engineering*

academicJournals